General Disclaimer

One or more of the Following Statements may affect this Document

- This document has been reproduced from the best copy furnished by the organizational source. It is being released in the interest of making available as much information as possible.

- This document may contain data, which exceeds the sheet parameters. It was furnished in this condition by the organizational source and is the best copy available.

- This document may contain tone-on-tone or color graphs, charts and/or pictures, which have been reproduced in black and white.

- This document is paginated as submitted by the original source.

- Portions of this document are not fully legible due to the historical nature of some of the material. However, it is the best reproduction available from the original submission.

Produced by the NASA Center for Aerospace Information (CASI)

CR 86293

NAS 12-667

FINAL REPORT ON

INVESTIGATION OF REFRACTORY DIELECTRIC FOR INTEGRATED CIRCUITS

By V. Y. Doo, P. J. Tsang, and P. C. Li

July 1969

Distribution of this report is provided in the interest of information exchange, and should not be construed as endorsement by NASA of the material presented. Responsibility for the contents resides with the organization that prepared it.

N70-14948 (ACCESSION NUMBER)
(THRU) 1
54 (PAGES)
(CODE) 09
NASA-CR-86293 (NASA CR OR TMX OR AD NUMBER)
(CATEGORY)
FACILITY FORM 602

Prepared under Contract No. NAS 12-667 by

INTERNATIONAL BUSINESS MACHINES CORPORATION

Hopewell Junction, New York 12533

ELECTRONICS RESEARCH CENTER

NATIONAL AERONAUTICS AND SPACE ADMINISTRATION

CAMBRIDGE, MASSACHUSETTS

NAS 12-667

FINAL REPORT ON

INVESTIGATION OF REFRACTORY DIELECTRIC FOR INTEGRATED CIRCUITS

By V. Y. Doo, P. J. Tsang, and P. C. Li

July 1969

Prepared under Contract No. NAS 12-667 by

INTERNATIONAL BUSINESS MACHINES CORPORATION

Hopewell Junction, New York 12533

ELECTRONICS RESEARCH CENTER

NATIONAL AERONAUTICS AND SPACE ADMINISTRATION

CAMBRIDGE, MASSACHUSETTS

1.0 SUMMARY

This is the final report for Contract No. NAS 12-667 describing the work performed during the contractural period from May 27, 1968 to May 26, 1969. Studies were conducted on Al_2O_3 growth on silicon or silicon oxide by chemical vapor deposition. Important parameters relating to the film growth including substrate temperature, source material composition, substrate preparation and carrier gases were investigated. Interfacial properties of the silicon-dielectrics concerning Al_2O_3 deposited on in-situ thermally or pyrolytically grown silica were studied. Selected property measurements included the flat band charge density before and after thermal bias treatment, dielectric strength and film refractive index. The masking capabilities of Al_2O_3 against common impurities of P, B, Ga, and Na were determined. Test IGFET devices using composite films of pyrolytic Al_2O_3 over thermal SiO_2 as gate insulators were successfully fabricated and their electrical performance was measured. In comparison with similar devices but using SiO_2 as gate insulators, Al_2O_3-SiO_2 have proven certain advantages, in particular it gives rise to a higher transconductance of the FET.

2.0 INTRODUCTION

With the advent of integrated circuits, the technology of thin dielectric film preparation by the chemical vapor deposition has made rapid progress in recent years. A comprehensive study[1] had been reported on pyrolytic insulators of silicon nitride and silicon oxynitride for integrated circuit application. These films exhibit many excellent properties including better diffusion masking capability, and thermal stability. Other comparable materials, however including pyrolytic Al_2O_3 and composite films of Al_2O_3 over SiO_2 for similar application have not been fully developed and thoroughly investigated. With the objective of further improving the reliability and stability of circuit elements for aerospace application and likewise in many other areas, this investigation was conducted aiming at the developing of basic information and understanding of these films in integrated circuit fabrication process. Based on experimental findings, the relative merits of selected dielectrics in circuit devices can be compared in terms of the fabrication techniques and device performance characteristics.

3.0 CHEMICAL VAPOR DEPOSITION OF Al_2O_3

Aluminum oxide film can be formed pyrolytically by either oxidation of organo-aluminum compounds or hydrolysis of aluminum halides. In this investigation anhydrous aluminum trichloride was chosen as the source material and the Al_2O_3 film was formed through the hydrolysis of $AlCl_3$ at elevated temperatures by the following reaction.

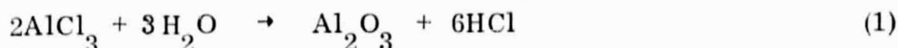

$$2AlCl_3 + 3H_2O \rightarrow Al_2O_3 + 6HCl \quad (1)$$

Under non-flow condition, the large positive values of the equilibrium constants of above equation (as shown in Fig. 1, equilibrium constant vs. reaction temperature) are always in favor of Al_2O_3 formation. If the water required for the above reaction is replaced with H_2 and CO_2, the deposition of Al_2O_3 can be modulated with ease. Since the reaction of H_2 and CO_2 proceeds rapidly at temperatures above 800^oC to furnish the needed water for $AlCl_3$, nucleation and growth of Al_2O_3 can occur only on the hot surface of the substrate, when the cold, mixed gases flow by it, and become heated high enough for water formation. Non-heated gases and reaction products are continuously swept out of the system by introducing a large quantity of diluent with the reactants. Consequently, heterogeneous reaction in the vapor phase for the following overall reaction would proceed in a very limited extent, if there is any.

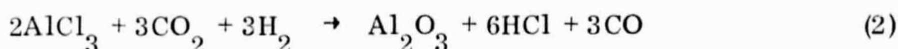

$$2AlCl_3 + 3CO_2 + 3H_2 \rightarrow Al_2O_3 + 6HCl + 3CO \quad (2)$$

Under such circumstances the film grown directly at the substrate surface would be most desirable. This type of film is expected to be homogeneous with least property variation in the microscopic scale. For convenience we call it the single mode of growth. On the contrary, if a substantially heterogeneous reaction takes place in the vapor phase rather than on the substrate surface, the resulting film would lack uniformity and its growth mode would be largely determined by the combined effect of both vapor phase and surface reactions. This type of film growth is differentiated from the other as bimodal growth. This generally occurs when the bulk gas stream is excessively heated to the temperature favorable for the reaction of H_2 and CO_2, appreciable water formed in the vapor phase would cause formation of aggregates which then condense on the substrate to form poor film.

In a flow reactor to be described latter in this report, the kinetics of Al_2O_3 formation is far more important. Unfortunately problems of this nature involving mass and energy transports accompanied simultaneously with chemical reactions is beyond the scope of this contract. Thus study in this area has to be limited to a few important parameters concerning the development of deposition process. Parameters of preliminary interest include the growth rate, growth mode and film morphology of Al_2O_3 with respect to temperature, type of diluent and the ratio of CO_2 to H_2 etc.

4.0 DESIGN AND CONSTRUCTION OF DEPOSITION SYSTEM

The deposition system for Al_2O_3 consists of three major parts, namely, the $AlCl_3$ evaporator, the gas feed system, and the reactor which is heated by a RF generator. The sketch shown in Fig. 2 is the general set-up for the system. The evaporator was made of a stainless steel pot with an air tight cover (Fig. 3).

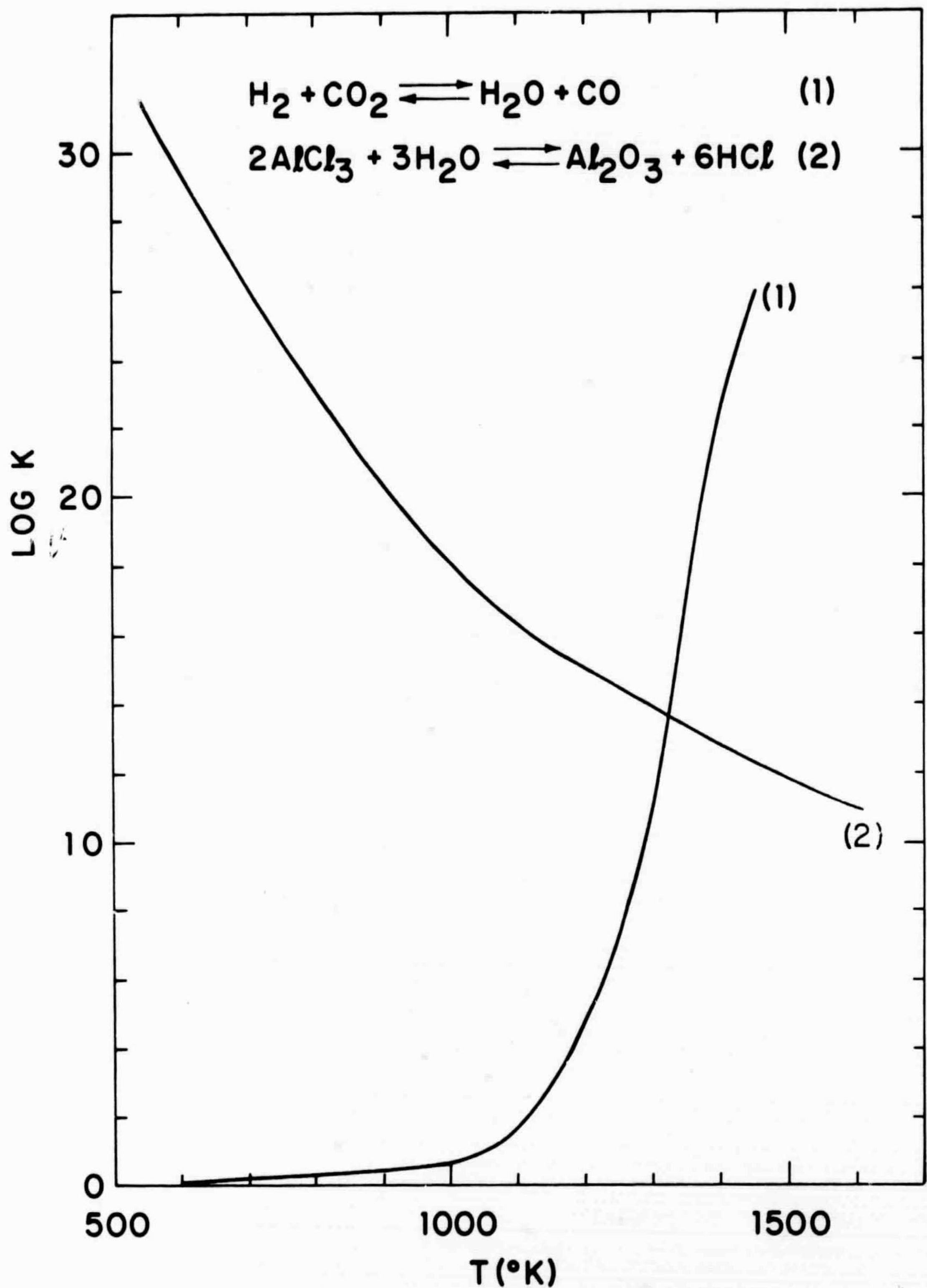

Fig. 1. Equilibrium constants of major chemical reactions as a function of reaction temperatures.

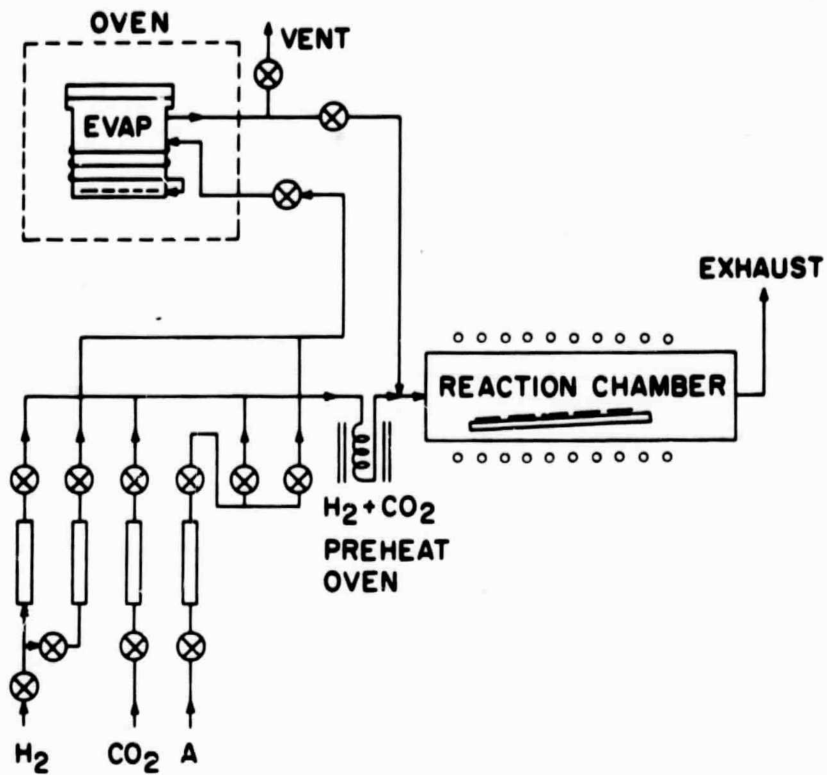

Fig. 2. System for pyrolytic Al_2O_3 deposition.

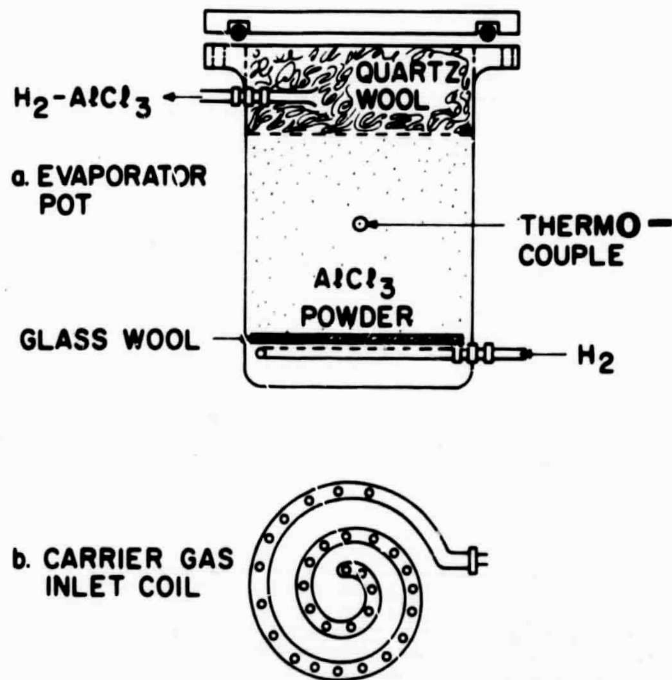

Fig. 3. $AlCl_3$ evaporator.

A perforated coil made of stainless steel was placed near the bottom of the evaporator for evenly distributing the incoming carrier gas (H_2) while the gas outlet port is situated near the top of the evaporator. To further insure even distribution of the incoming carrier gas and to prevent $AlCl_3$ powder from falling down and blocking the openings, a thin layer of predried glass wool was placed right on the top of the perforated stainless steel coil. The powder was then loaded above the glass wool. Loading and unloading of the powder can be made through the top of the evaporator with the airtight cover removed. After the powder was loaded, a thick layer of moisture-free quartz wool was placed loosely on the top of the $AlCl_3$ powder but just below the $AlCl_3$ vapor outlet port to prevent any dust from entering the feed line. To vaporize $AlCl_3$, the evaporator was placed in an oven maintained at a constant temperature, 115°C.

The gas system was so designed that the gaseous reactants H_2 and CO_2 would meet and thoroughly mix with the $AlCl_3$ vapor (carried by a small flow of H_2) before entering the reactor. An argon line was provided to supply argon gas for flushing. All the eed lines thermally insulated to prevent condensation of $AlCl_3$ vapor. In addition, the gaseous reactants H_2 and CO_2 were preheated before mixing with the $AlCl_3$ vapor and entering the reactor.

The reactor itself was made of fused quartz tube 2.5" in diameter. A silicon carbide coated graphite slab, heated by a RF coil, was used as sample holder and also as susceptor.

The major difficulty of the system in the earlier stage was the condensation of $AlCl_3$ vapor which leads to clogging of the lines. To eliminate this problem the feed system was later modified to provide adequate thermal protection to the entire feed line. All feed lines in the system were heated at least 15°C to 20°C higher than that of the evaporator temperature. Another difficulty encountered was the building-up of unstable pressure in the evaporator. This was overcome later by replacing all the slip valves with straight opening valves.

5.0 MATERIALS AND DEPOSITION PROCEDURE

Materials available in high purity were chosen for the Al_2O_3 deposition, including anhydrous $AlCl_3$ powder, electronic grade CO_2 gas, in-house purified H_2 (99.9985% purity) and Ar (99.998% purity).

During the film deposition the following procedures were generally observed:

1. Flush the system and reaction chamber by argon gas for 15 minutes.

2. Flush the system and reaction chamber by hydrogen gas for 15 minutes.

3. Turn on RF power, the substrate was then heated to the desired temperature. Depending on the final chosen substrate temperature, usually 10 to 15 minutes was needed to stabilize the temperature.

4. Inject CO_2 15 seconds prior to the injection of $AlCl_3$ vapor.

5. Inject $AlCl_3$ vapor.

At the end of deposition, the following steps were performed in sequence:

6. Stop $AlCl_3$ vapor injection.

7. After approximately 15 seconds the injection of CO_2 is stopped.

8. One minute later, the RF power is turned off. Substrates are allowed to cool-down to room temperature in the reactor under hydrogen atmosphere.

During the initial study, only the substrate temperature was chosen as a variable while keeping other conditions constant. The $AlCl_3$ evaporator was kept at 115°C at which a vapor pressure of 4.5 mmHg of $AlCl_3$ may be obtained.[2] Since a large amount of H_2 was used as the main carrier gas, the feed rate of CO_2 would be essentially determining the mode of chemical reaction at any given substrate temperature consequently predominating the film growth mode. In the initial series of runs, excessive amounts of CO_2 were introduced to assure that there would be adequate water in the system for complete hydrolysis of $AlCl_3$.

The representative deposition conditions for Al_2O_3 films are shown in Table I.

6.0 GROWTH MODE AND FILM MORPHOLOGY

For integrated circuits application, the dielectric films must be physically homogeneous and free from pin holes or structural defects, all of which can cause device instability. It is highly desirable to have a film of single phase so that the film properties, both physical and chemical, can maintain uniformity in every micro-spot. This requirement is extremely important to the reliability of electronic device.

Al_2O_3 films were chemically deposited under the general deposition conditions in Section 5.0.Their growth mode was analyzed and the film morphology was determined.

In general, films grown at 850°C or lower are characterized by having a clear shiny surface which shows only a few "white spots" under the dark field of a metallographic microscope. If examined under a phase contrast microscope, the surface of the film looks as if it were composed of tiny spherical grains (Fig. 4).

TABLE I. General Deposition Conditions

H_2 (main carrier gas)	20 1./min.
H_2 ($AlCl_3$ vapor carrier gas)	150 cc/min.
CO_2	400 cc/min.
$AlCl_3$ evaporator temperature	115°C
$AlCl_3$ feed line temperature	140°C
H_2 (main carrier gas) + CO_2 pre-heat temperature	140°C
Substrate temperature	Varies

The grain size roughly depends on the substrate temperature. The higher the substrate temperature, the larger the grain, hence the coarser the surface appearance. It is evident that below 850°C the relatively slow water formation rate tends to give rise to a homogeneous gas phase reaction. However, the possibility of having some heterogeneous reaction can not be completely excluded due to the presence of excessive CO_2 which can enhance the water formation. Therefore below 850°C although the film is dominated by an epitaxial-like growth, the film matrix containing some dispersed grains may be still observed. This is attributed to the premature reaction occurred in the vapor phase. When the substrate temperature was raised above 900°C, the heterogeneous-gas phase reaction became so prominent that tiny cubic crystallites imbedded in the continuous matrix film were observed. Cubic γ - Al_2O_3 crystallites were often observed in the films grown at temperatures between 900°C to 1000°C while needle like α - Al_2O_3 crystallites were identified in the films grown at 1100°C. When the grains were large, the films appear less shiny and become milky, showing white spotty clouds as typical surface texture under the dark field microscope. Films appear quite hazy when they contain a large amount of heterogeneously grown crystallites. In summary, when an excessive amount of CO_2 is present, the film growth is dominated by a chemical reaction at the substrate surface below the temperature of 850°C, whereas at temperatures higher than 850°C, it is likely to be dominated by the heterogeneous reaction in the gas phase.

7.0 FILM STRUCTURE

The structure of Al_2O_3 films was examined by an electron microscope. Glancing electron diffraction revealed that all the films deposited at temperatures higher than 700°C were polycrystalline, except a few films deposited at 900°C and 1000°C with a single crystal structure. (Figs. 5, 6) The grain size ranged from 200Å to 1000Å, depending upon the substrate temperature. Some line broadening of the electronic diffraction patterns of films deposited at 700°C and 750°C was observed indicating the existence of amorphous phase. The structure of 900°C and 1000°C films showed strong preferred orientation with {110} in parallel to the substrate surface of {100} orientation (Fig. 5), and some even showed epitaxially grown single crystal of γ - Al_2O_3 pattern on (111) Si substrate (Fig. 6). In general, the crystal structure of the film as a function of the deposition temperature may be summarized as:

Substrate Temp. (°C)	700	800	900	1000	1100
Al_2O_3 Structure					
Major phase	Amorphous	κ	γ	γ	$\gamma + \alpha$
Minor phase	κ	γ	κ	α	

The present observation of the structural change with the deposition temperature is more or less comparable with the process of dehydration of boehmite,[3] namely the formation of partially dehydrated boehmite at temperatures lower than

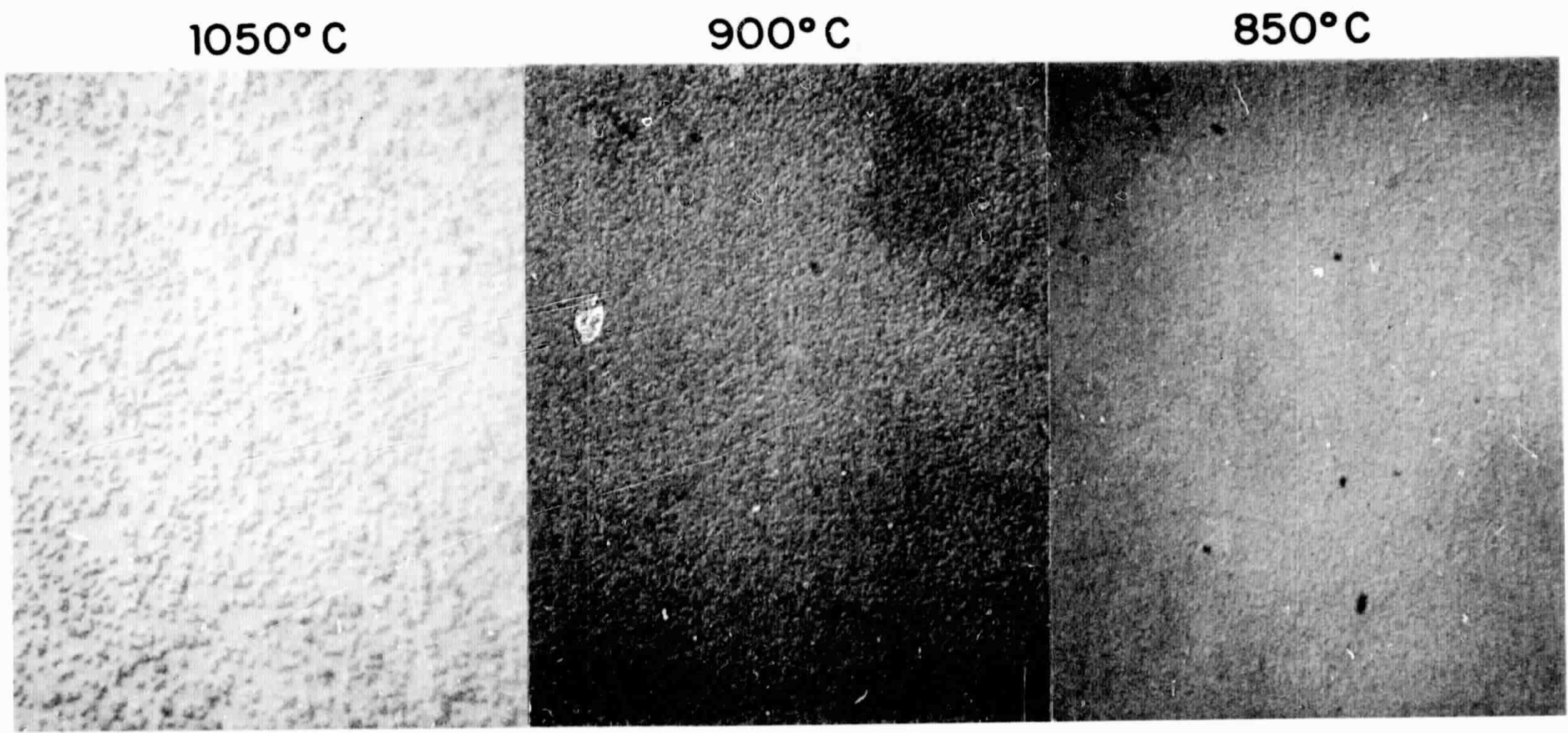

Fig. 4. Surface structure of films grown at various temperatures revealed by phase contrast microscope. Note film grown at 1050°C was full of cubic crystallites which were tentatively identified as being α-Al_2O_3.

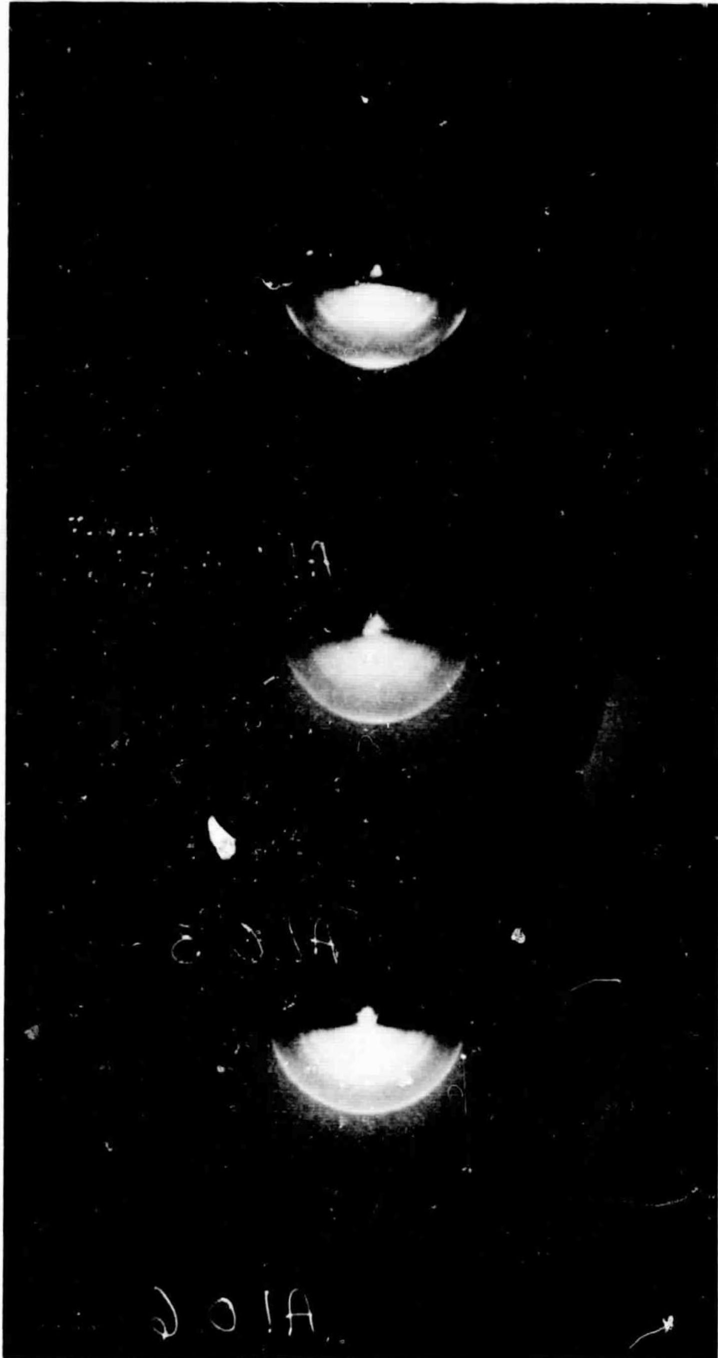

Fig. 5. Glancing electron diffraction pattern of some Al_2O_3 films deposited at 900°C.

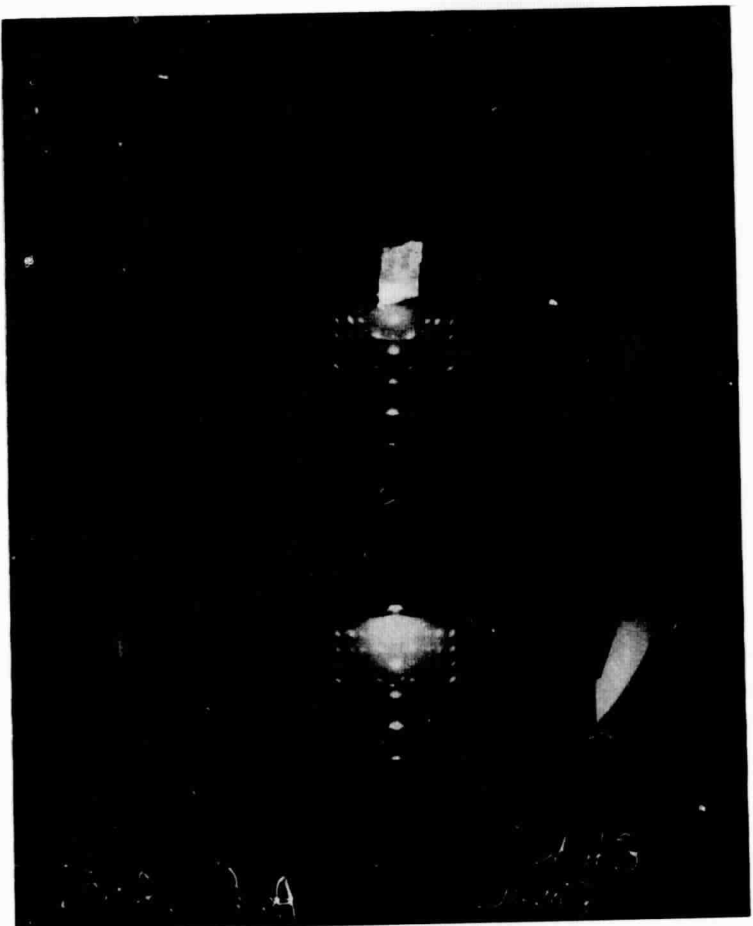

Fig. 6. Glancing electron diffraction pattern of sample 12-5. Epitaxial single crystal pattern was identified as γ-Al_2O_3. Top picture shows the structure of the film as deposited while the lower picture shows the structure of the same film after a very thin top surface layer was removed.

$800^{o}C$. As the deposition temperature increases, a transition from κ - Al_2O_3 to metastable γ - Al_2O_3 and finally to stable α - Al_2O_3 occurs. There is no clear-cut demarcation between transitions. However, in general, the $\kappa \rightarrow \gamma$ transition occurred around $800^{o}C$ while the $\gamma \rightarrow \alpha$ transition occurred around $1000^{o}C$.

8.0 FURTHER STUDIES OF GROWTH MODE AND MORPHOLOGY OF Al_2O_3 FILM AT $900^{o}C$

For microelectronics applications, homogeneous, single modal, single phase insulating films are most desirable. In addition, the film deposition temperature should be as low as possible. Results obtained from earlier study shows that the homogeneous single modal γ phase Al_2O_3 film was formed at $900^{o}C$ under suitable deposition conditions. Therefore, the effect of other process parameters on the growth mode and morphology of the films were further studied at $900^{o}C$.

8.1 Effect of $CO_2/AlCl_3$ Mole Ratio on the Growth Mode of Al_2O_3

In this section the mode and growth rate of Al_2O_3 film were carefully studied at $900^{o}C$ as a function of the $CO_2/AlCl_3$ mole ratio. This temperature was chosen because of the well identified γ phase Al_2O_3 film formation. By maintaining constant flow of main carrier gas (H_2) and the carrier gas for $AlCl_3$ (H_2) (20 1/min and 500 cc/min, respectively), the $CO_2/AlCl_3$ mole ratio was varied from 15:1 to 90:1 by changing the CO_2 flow rate.

Experimental results are presented in Fig. 7, in which the film growth rate steadily increases with an increasing $CO_2/AlCl_3$ mole ratio. At low mole ratio of $CO_2/AlCl_3$, the Al_2O_3 films were visually clear, indicating a single mode of growth. However, if the $CO_2/AlCl_3$ ratio was increased excessively, a bimodal film formed. When excess CO_2 is contained in the gas phase, the amount of water formed can be sufficiently high to cause a pronounced Al_2O_3 formation in the gas phase rather than on the substrate surface. Experience from experimental observation indicates that the ratio of $CO_2/AlCl_3$ approximately at 20:1 appears most satisfactory in the existing system.

8.2 Effect of $AlCl_3$ Concentration on the Growth of Al_2O_3 Film

The ratio of main carrier gas over $AlCl_3$ carrier gas is another factor to control the reaction rate. The higher the main carrier gas flow rate, the less the concentration of $AlCl_3$ in the gas phase thus lowering the reaction rate. At $900^{o}C$, the satisfactory ratio of main carrier gas over $AlCl_3$ carrier gas is approximately 30:1 when the $AlCl_3$ vaporized at $115^{o}C$. If the substrate is heated to a higher temperature, this ratio must be increased correspondingly, other-

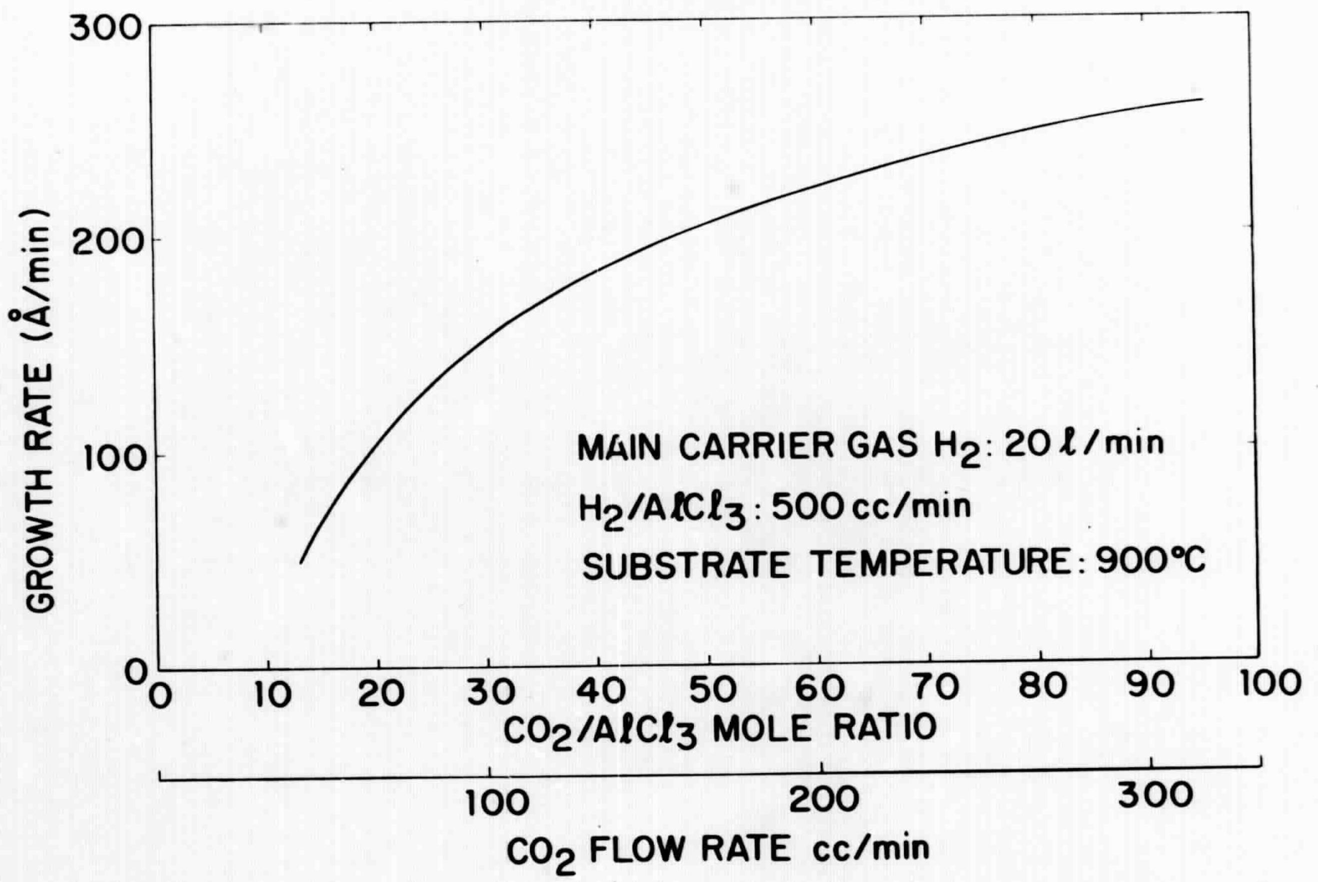

Fig. 7. Effect of $CO_2/AlCl_3$ mole ratio on the growth of Al_2O_3 film on silicon wafer.

wise a single modal film growth would not be maintained. This is illustrated by the following example. At 1000°C and $CO_2/AlCl_3$ = 18:1, the Al_2O_3 film prepared was found to be of bimodal growth under the ratio within 70 for the main carrier gas over $AlCl_3$ carrier gas. But when this ratio was doubled, the film appeared to be of single modal growth. Thus, at high deposition temperature, it is important to properly dilute the $AlCl_3$ concentration to prevent any possible early formation of Al_2O_3 in the gas phase.

8.3 Effect of Argon Gas on the Growth of Al_2O_3 Film

A study was conducted by substituting A for H_2 as the main carrier gas. It was found that the complete substitution of A for H_2 tends to substantially decrease the film growth rate from ~ 150 Å/min. to ~20 Å/min., when other conditions were kept unchanged.

When a mixture of H_2 and A was admitted as the main carrier gas, the growth rate of the Al_2O_3 film increased. Results indicated that the growth rate of Al_2O_3 film increases linearly with increasing H_2 concentrations in the gas phase as shown in Fig. 8. High A concentration appears to produce two effects. First, the gas phase reaction seems to be depressed; and second, the single modal growth is likely to extend to a higher substrate temperature. The stoichiometry of the Al_2O_3 may differ when using H_2 as the sole carrier gas. This sort of speculation needs additional experimental study.

8.4 Effect of Helium Gas on the Growth of Al_2O_3 Film

The effect of He on Al_2O_3 film was investigated. It was found that the film growth rate decreases linearly with increasing He content in the main carrier gas. Results are shown in Fig. 9, in which the He content was varied from 10% to 90% and the respective growth rate varying from 95 to 40 Å/min. The film quality appears poor and non-uniform when the He content exceeded 90%. Its refractive index is approximately 1.745 independent of He content in the carrier gas.

9.0 STRUCTURAL COMPARISONS OF Al_2O_3 FILM DEPOSITED ON OXIDIZED AND NON-OXIDIZED Si SUBSTRATES

The structure and appearance of the Al_2O_3 films deposited on oxidized Si substrates differed markedly from that on bare Si-substrates. The amorphous-crystalline phase transition temperature of the Al_2O_3 films deposited on oxidized Si is higher than those deposited on bare Si because of the structural difference in substrates. For the same reason, single crystal Al_2O_3 film was never observed on oxidized substrates even though preferential orientation has been found in some films.

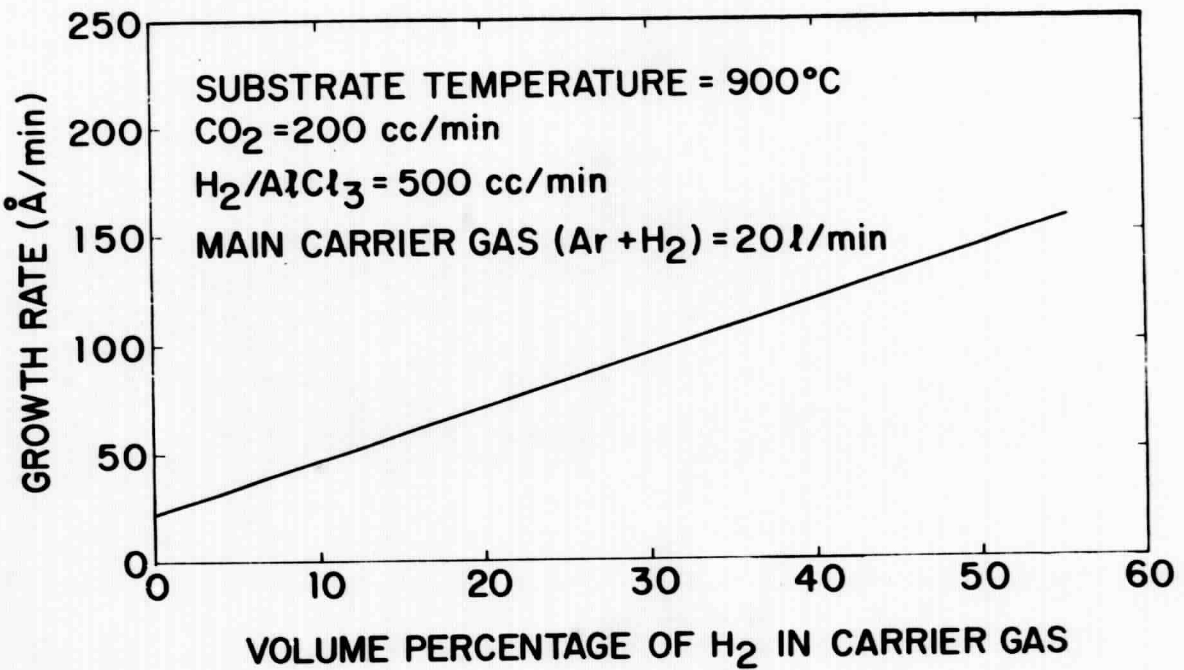

Fig. 8. Effect of composition of carrier gas on Al_2O_3 film growth.

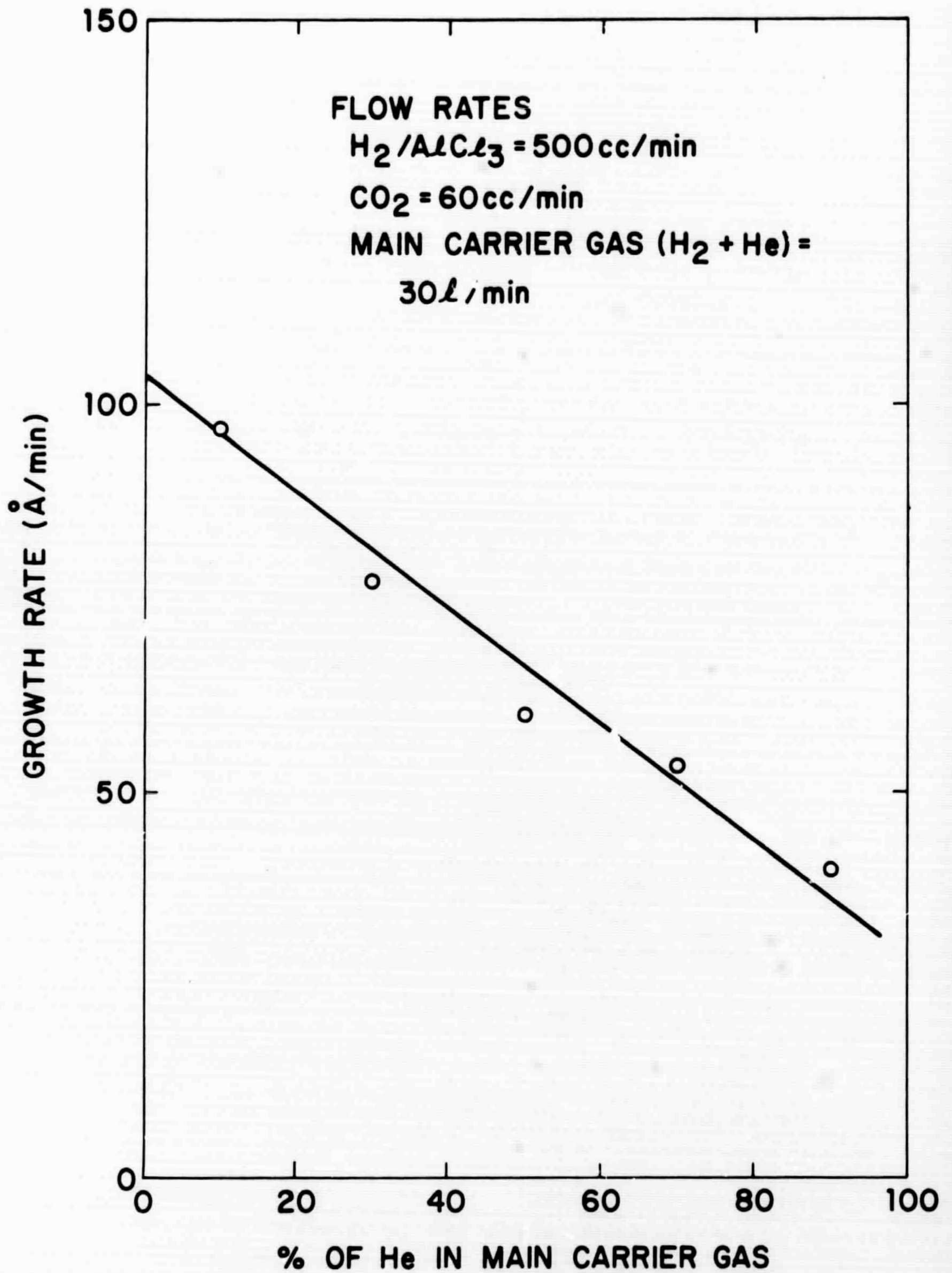

Fig. 9. Effect of substituting of He for H_2 as main carrier gas on the growth rate of the Al_2O_3 film.

The topograph of the Al_2O_3 films deposited at different temperatures on oxidized and bare Si substrates was investigated by using the scanning electron microscope, SEM. Samples a1, b1 and c1 were deposited on bare Si substrates and a2, b2, and c2 on oxidized substrates. The deposition temperature for samples a1 and a2 was 1050°C, b1 and b2 at 900°C, and c1 and c2 at 700°C. Figure 10 shows the SEM topograph magnification at 100 and Fig. 11 at 10,000. Note in Fig. 10, that all samples appear to be smooth. However, under high magnification, the topographs differed markedly from one sample to another. In general, high surface asperity was observed on films deposited at high temperature and on oxidized substrates. A sectional SEM micrograph of a 2.5μ film grown at 1100°C was shown in Fig. 12. Its columnar grain structure typical of thick films of pyrolytic materials is readily observable.

10.0 GROWTH RATES OF Al_2O_3 FILMS

The growth rate of Al_2O_3 film was studied as a function of substrate temperature and $AlCl_3$ injection rate. In Fig. 13, the Al_2O_3 film growth rate is plotted against the reciprocal of absolute deposition temperatures. The sharp break at approximately 850°C suggests that two distinctive film growth mechanisms may exist in the temperature range of 700°C to 1100°C. The apparent activation energy for the deposition in the lower temperature range is about four times as large as that in the higher temperature range. At lower deposition temperatures it is possible that the surface reaction is responsible for the film growth thus requiring higher activation energy. Whereas, at higher temperatures the condensation of Al_2O_3 from the gas phase appears dominating the film growth.

The growth rates were also studied at 750°C and 1000°C as a function of the amount of $AlCl_3$ vapor introduced into the reaction chamber with the CO_2 injection rate kept constant. At 750°C, the film growth rate, after a short incubation period, was more or less independent of the injection rate of $AlCl_3$ vapor, indicating the H_2O formation rate as a limiting factor to the film growth. On the other hand the deposition rate at 1000°C increased continuously with increasing $AlCl_3$ injection rate, confirming that the condensation of Al_2O_3 from the gas phase predominated the film growth at high temperatures. The growth rates at respective temperatures 750° and 1000°C as a function of $AlCl_3$ feed rate were shown in Fig. 14.

11.0 GENERAL PROPERTIES OF Al_2O_3 FILMS

11.1 Etching Rates in Hot Phosphoric Acid

Al_2O_3 films grown at 700°C and 750°C dissolve readily in hot phosphoric acid. The etching rates were too fast to be measured. Etching rates of films grown at other temperatures are shown in Fig. 13. As illustrated, 850°C seems to be a transition temperature.

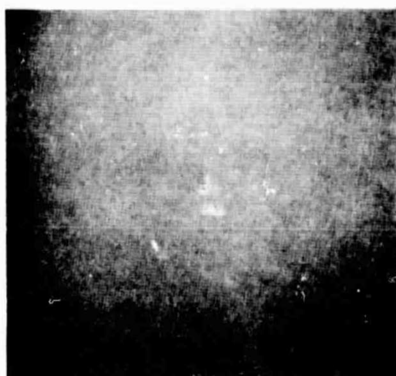

a1 60-3 100X

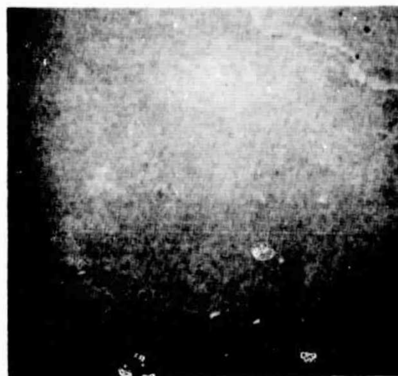

a2 60-6 100X

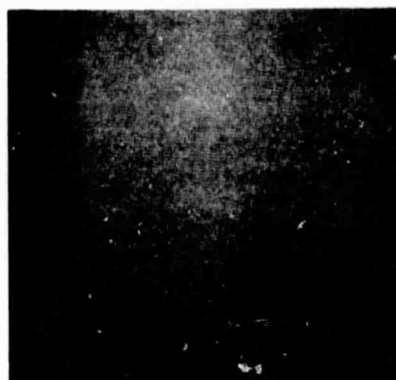

b1 66-7 100X

b2 66-6 100X

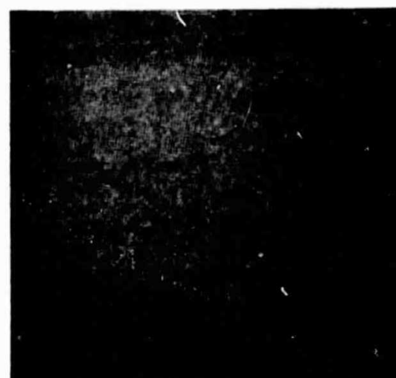

c1 54-3 100X

c2 54-7 100X

Fig. 10. SEM micrographs of the surface of Al_2O_3 films deposited at various temperatures. Magnifications X100. a1 and a2 deposited at 1050°C; b1 and b2 deposited at 900°C; c1 and c2 deposited at 700°C. a1, b1 and c1 without SiO_2 underlayer; a2, b2 and c2 with SiO_2 underlayer.

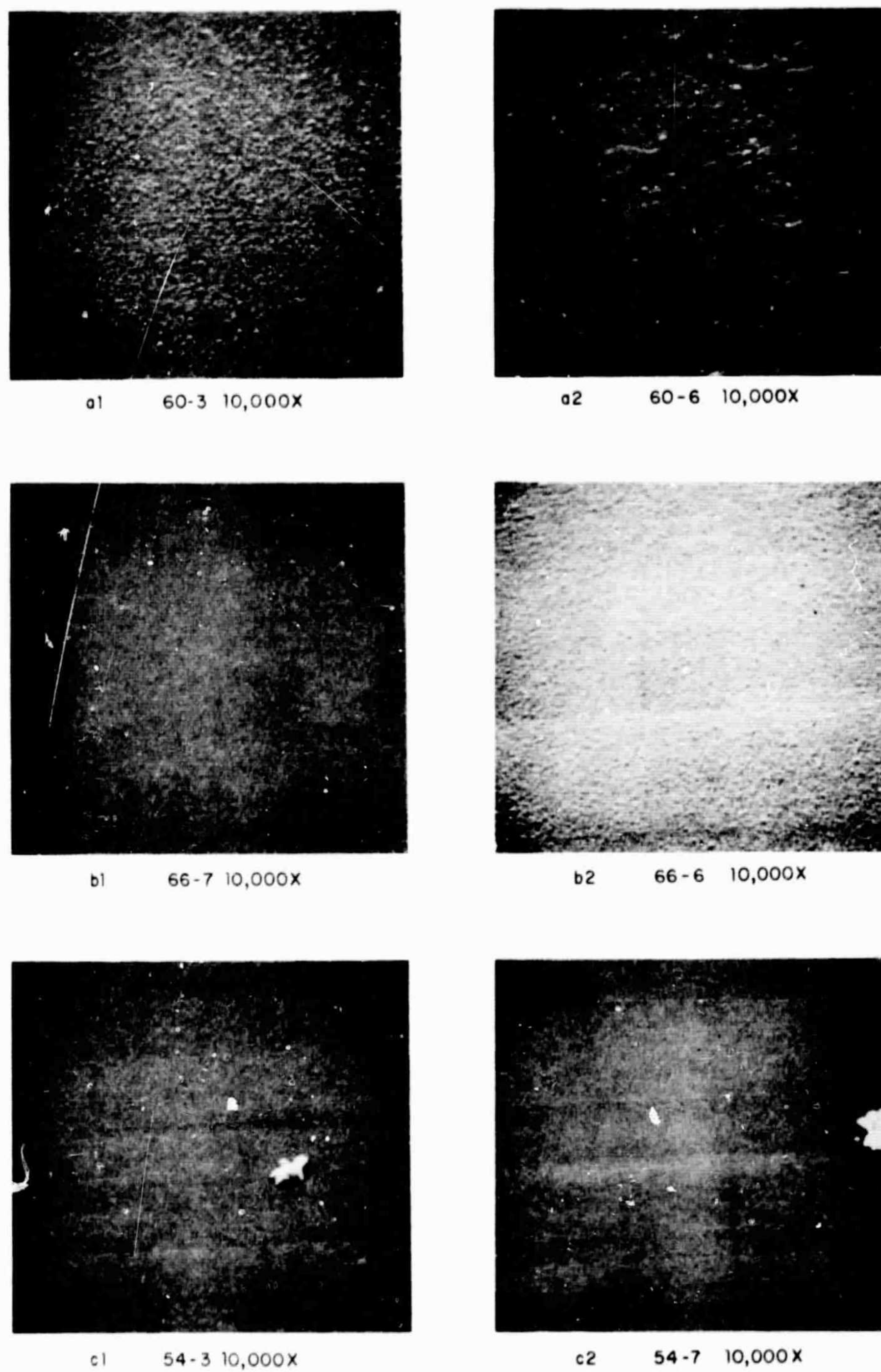

Fig. 11. SEM micrographs of the surface of Al_2O_3 films. Same as that shown in Fig. 4 but at much higher magnification: X10,000.
a1 and a2 deposited at 1050°C, b1 and b2 deposited at 900°C; c1 and c2 deposited at 700°C.
a1, b1, and c1 without SiO_2 underlayer; a2, b2, and c2 with SiO_2 underlayer.

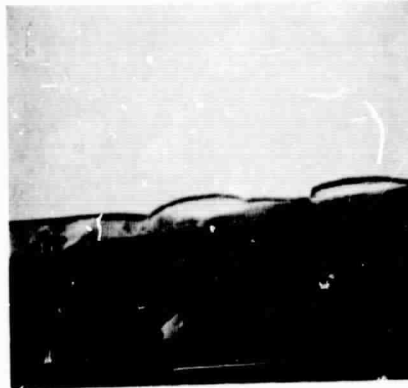

80 200X

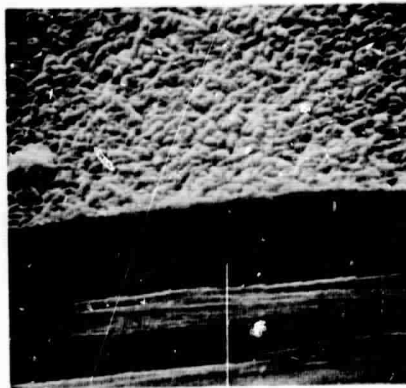

80 2400X

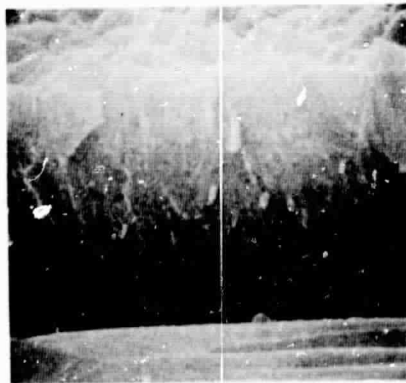

80 12,000X

Fig. 12. SEM micrographs of the cross-section of a thick Al_2O_3 film deposited at $1100^\circ C$.

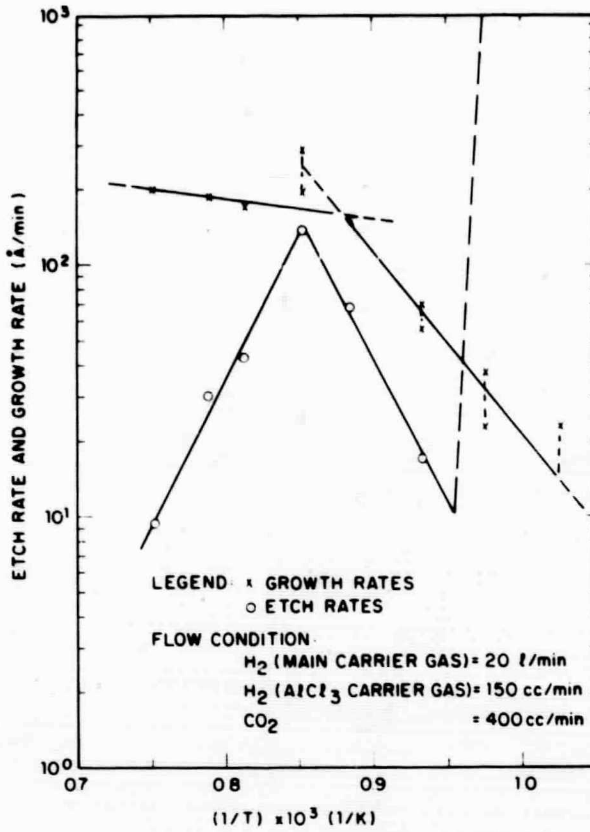

Fig. 13. Growth rates vs. deposition temperatures.

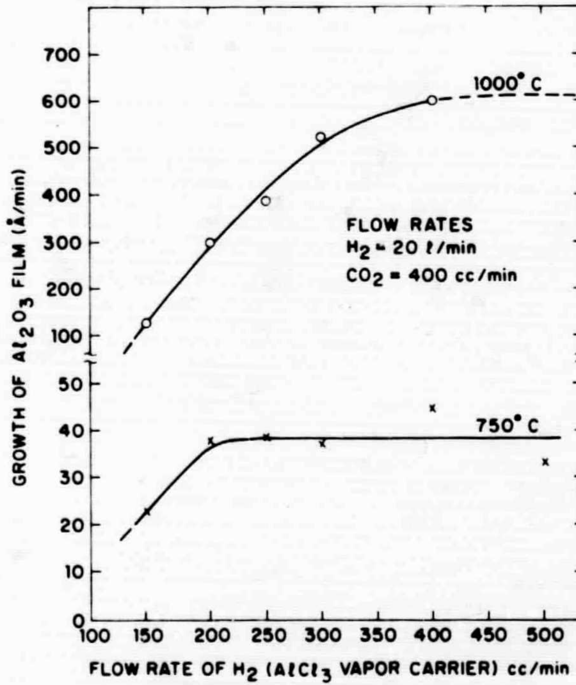

Fig. 14. Growth rate of Al_2O_3 film as a function of $AlCl_3$ flow rate.

11.2 Etching Rate in 48% HF Solution

Films grown at 700°C and 750°C dissolve in 48% HF readily. However, all the films grown at temperatures higher than 800°C were practically non-etchable by 48% HF. Films left in HF folution for 110 minutes at room temperature show no signs of being attacked.

11.3 Index of Refraction

Index of refraction, n, of the Al_2O_3 films deposited at various temperatures were measured by ellipsometer. In general, the index of refraction of the films deposited at or below 750°C was found to be 1.66 while it was found to be 1.73 to 1.76 for the films deposited at or above 800°C. No general relation between the deposition temperature and the index of refraction of the Al_2O_3 film could be found.

11.4 Dielectric Constants and Dielectric Strength

The dielectric constants, K, of Al_2O_3 films were calculated from the capacitance of the MAS measurements. With the exception of 800°C film where k = 20, the dielectric constants of Al_2O_3 films are in the range of 6.8 to 11.0 with a statistical maximum at 10.0 and appear to be independent on the deposition temperature. The variation in K values of Al_2O_3 film might be attributed to the difference in degree of preferential orientation and the extent of crystal imperfections. The dielectric breakdown strength of the Al_2O_3 films is approximately 9×10^6/cm or higher. This breakdown strength does not appear to bear any quantitative relationship with the substrate temperatures.

11.5 Infrared Spectra

The infrared transmission spectra of the films deposited at various temperatures were measured by Beckman IR-10. Results are shown in Fig. 15 absorption bands beyond 11.0μ are observed, which agrees with the findings of Harris.[4] It is noted that the films deposited at higher temperatures show several strong peaks, in particular at 13μ, 19.8μ, and 29μ. These peaks are generally absent in the spectrum of sputtered amorphous Al_2O_3 films.[5]

11.6 UV Absorption Spectrum

An UV absorption spectrum of film deposited on a quartz disk at 750°C was taken using Beckman DK-2. It shows a strong absorption band around 1880Å with the high energy edge at about 1820Å and a prolonged low energy tail extended to 1950Å. Two weak absorption bands peaked at 2700Å and 4250Å, respectively, were also observed.

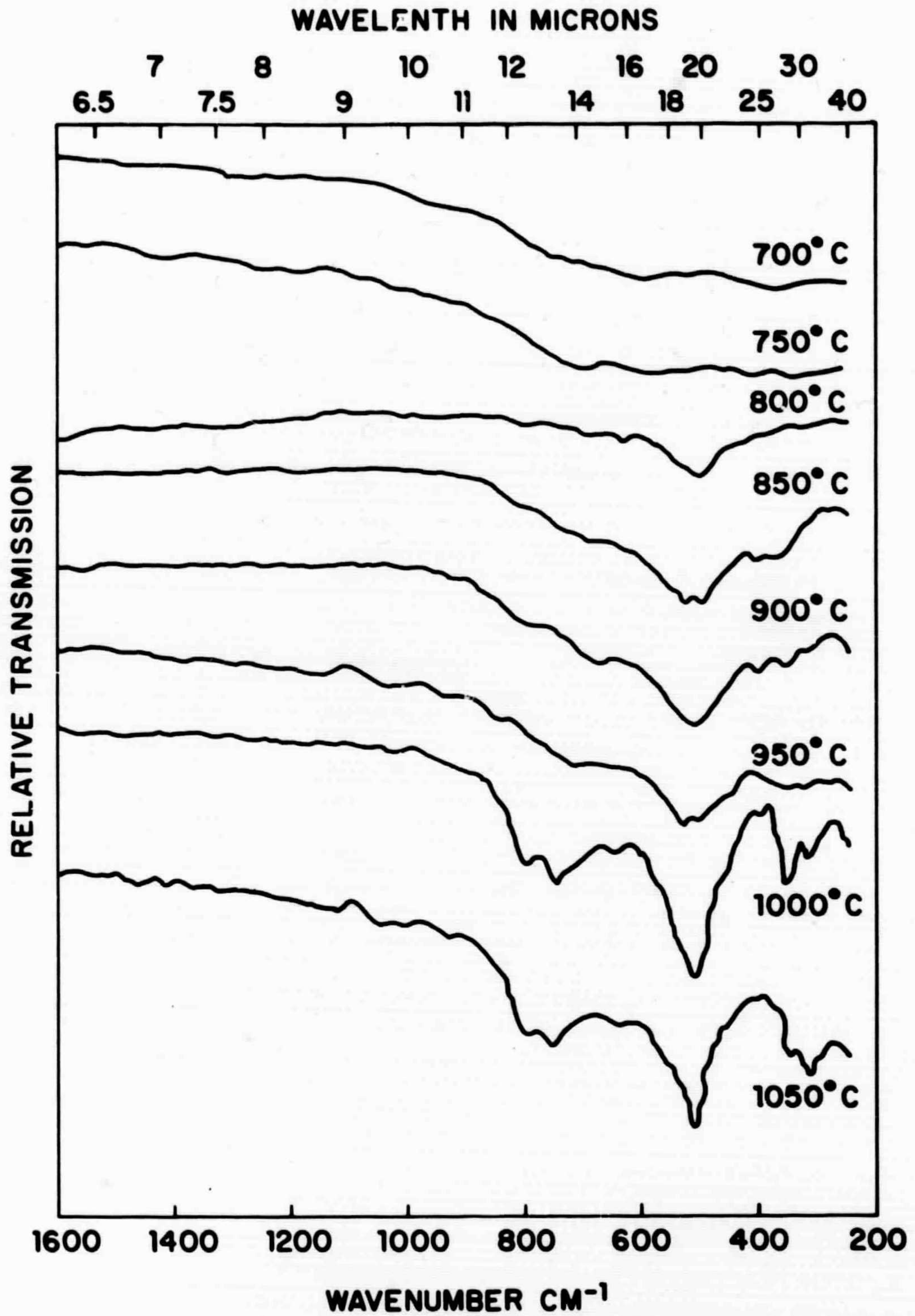

Fig. 15. Infrared absorption spectrum of pyrolytic Al_2O_3 films deposited at various temperatures.

11.7 Diffusion Masking Effect

The masking effect of Al_2O_3 film prepared at 900°C against the diffusion of common dopants such as P, B, and Ga was investigated. Diffusion was carried out individually in sealed capsules for 70 minutes at 1050°C for P, 60 minutes at 1100°C for B, and 70 minutes at 1100°C for Ga. Diffused junction depth was determined by the bevel-delineation method. Several Al_2O_3 thicknesses were used for each diffusion species. The results are shown in Fig. 16. The Al_2O_3 films, effectively masked P-diffusion but not the B-& Ga-diffusion. Thick Al_2O_3 films did not help mask B-& Ga-diffusion because thick films tend to have a well defined columnar grain structure. The preferred grain boundary diffusion suggested a rugged junction as shown in Fig. 16.

12.0 Na RETAINING ABILITY OF Al_2O_3 FILMS

Two samples consisting of composite films of Al_2O_3 -SiO_2 were prepared. One sample designated as 12 Al has 4500Å thermal SiO_2 and 1000Å Al_2O_3 and the other, 7 Al has 800Å thermal SiO_2 and 1200Å Al_2O_3. These samples were then deposited with NaCl so that the surface concentration of Na contamination was approximately 10^{13} atoms/cm^2. This was done by first evaporating 0.5 ml of 0.0005 mole NaCl solution in a tungsten boat and then vacuum vaporizing the salt onto the films. Finally the MAOS samples were prepared using Al metallurgy as done by standard methods. The V_{FB} and N_{FB} of these samples were calculated from the measured C-V curves under temperature bias treatments. Results were presented in Table II. Data indicated that these Na contaminated samples tend to increase the negative V_{FB}, independent of the film thickness. As compared with the data from non-contaminated samples prepared in runs 10 Al and 5 Al-2 having comparable film thickness as 12 Al and 7 Al, respectively, the increment of negative V_{FB} of these Na contaminated samples is approximately 3 volts. Consequently there is an increase of negative surface charge at the silicon surface of about 6×10^{11} charge/cm^2. It is further noticed that both V_{FB} and N_{FB} of these Na contaminated samples did not show any substantial change even after prolonged heat treatments, indicative of excellent film stability. After these samples were under temperature bias treatments (applied voltages ranging from ± 5 to ± 30), the thin composite film (7 Al) was found to have a maximum V_{FB} shift of - 1.4V and the thick composite (12 Al), - 3.0V. The change of surface charge density, $(-\Delta N_{FB})$, for both samples were in the order of 10^{11} charge/cm^2. Results from above measurements strongly suggest the low mobility and high retaining ability of Na ions in Al_2O_3 film. These results confirm previous finding in the Na isotope diffusion experiment.[16]

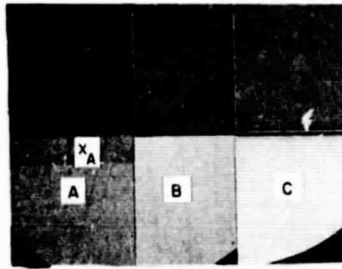

P DIFFUSION
$X_A = 1.96\ \mu$

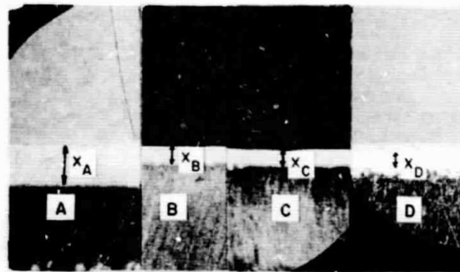

Ga DIFFUSION
$X_A = 2.4\mu$ $X_B = 1.19\mu$; $X_C = 1.13\mu$; $X_D = 1.20\mu$

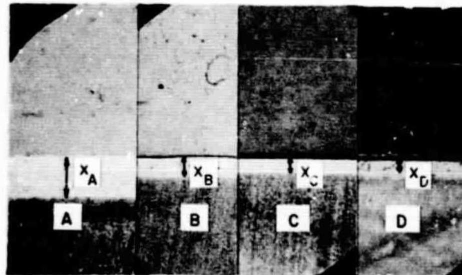

B DIFFUSION
$X_A = 2.6\mu$; $X_B = 1.23\mu$; $X_C = 1.37\mu$; $X_D = 1.35\mu$

Fig. 16. Microphotographs of the beveled and stained cross-section of silicon wafers, with or without Al_2O_3 covered, after diffusion treatment.

Photo (1). Phosphorous capsule diffusion. A. blank wafer; B. 1500Å Al_2O_3 covered; C. 3300Å Al_2O_3 covered.

Photo (2). Gallium capsule diffusion. A. B, C. Same as photo (1). D. 5300Å Al_2O_3 covered

Photo (3). Boron capsule diffusion. A, B, C, D. Same as photo (2).

TABLE II. V_{FB} and N_{FB} of Na-Contaminated Samples.

A. Sample 12 Al, 1000 Å Al_2O_3 + 4500 Å Thermal SiO_2

No. of Test Sequence	Temp. - Bias Test (in dry N_2) Temp./Time	Bias	V_{FB} (V)	N_{FB} (charge/cm^2)	ΔV_{FB} (V)	ΔN_{FB} (charge/cm^2)
1	As Received and Na Contaminated		-6.5	-3.14×10^{11}	-3.2^{*}	-4.4×10^{10} *
2	200°C/30 min.	0	-6.0	-2.74×10^{11}	$+0.5^{**}$	$+4.0 \times 10^{10}$ **
	200°C/30 min.	+5	-7.8	-3.56×10^{11}	-1.8	-8.2×10^{10}
3	200°C/30 min.	0	-6.0	-2.99×10^{11}	-0.0^{**}	-2.5×10^{10}**
	200°C/30 min.	+30	-9.0	-4.49×10^{11}	-3.0	-15.0×10^{10}
4	200°C/30 min.	0	-6.0	-2.79×10^{11}	-0.0^{**}	-0.5×10^{10}**
	200°C/30 min.	-5	-6.0	-2.79×10^{11}	-0.0	-0.5×10^{10}
5	200°C/30 min.	0	-6.0	-2.79×10^{11}	-0.0^{**}	-0.5×10^{10}**
	200°C/30 min.	-30	-6.0	-2.79×10^{11}	-0.0	-0.5×10^{10}
6	200°C/150 min.	0	-7.8	-3.56×10^{11}	-1.8^{**}	-8.2×10^{10} **
	200°C/150 min.	+30.0	-7.8	-3.56×10^{11}	0.0	0.0
7	200°C/150 min.	0	-7.8	-3.56×10^{11}	0.0^{**}	0.0^{**}
	200°C/150 min.	-30.0	-6.0	-2.79×10^{11}	+1.8	$+8.2 \times 10^{10}$

*Compared with the V_{FB} and N_{FB} of Non-Na contaminated Sample 10 Al which has V_{FB} and N_{FB} of -3.3V and -2.7×10^{11} charge/cm^2, respectively.

**Compared with the corresponding values of those of as received Na-contaminated sample.

B. Sample 7 Al 1200 Å Al_2O_3 + 800 Å Thermal SiO_2

No. of Test Sequence	Temp./Time	Bias	V_{FB} (V)	N_{FB} (charge/cm^2)	ΔV_{FB} (V)	ΔN_{FB} (charge/cm^2)
1	As received No T-B Test		-4.2	-7.03×10^{11}	-3.16^{*}	-5.03×10^{11} *
2	200°C/30 min.	No	-4.0	-6.34×10^{11}	$+0.2^{**}$	$+6.9 \times 10^{10}$ **
	200°C/30 min.	+5	-4.2	-6.8×10^{11}	-0.2	-5.4×10^{10}
3	200°C/30 min.	No	-3.7	-6.06×10^{11}	$+0.5^{**}$	$+9.7 \times 10^{10}$
	200°C/30 min.	+30	-5.1	-8.37×10^{11}	-1.4	-2.3×10^{11}
4	200°C/150 min.	No	-4.2	-7.00×10^{11}	0.0^{**}	$+3.0 \times 10^{9}$ **
	200°C/150 min.	+30	-5.5	-8.79×10^{11}	-1.3	-1.79×10^{11}

*Compared with the V_{FB} and N_{FB} of Non-Na contaminated Sample 5 Al-2, which has V_{FB} and N_{FB} of -1.04 V and 2.0×10^{11}, respectively.

**Compared with the corresponding values of those of as received Na-contaminated sample.

13.0 SURFACE CHARGE OF MAS ($Al-Al_2O_3-Si$) AND MAOS ($Al-Al_2O_3-SiO_2-Si$) SYSTEMS

The insulator-semiconductor interfacial charge property of MAS and MAOS systems has been studied by measuring the C-V characteristocs of MAS and MAOS capacitors.[6] The surface charge densities of these two systems were studied as functions of substrate temperature, $CO_2/AlCl_3$ mole ratio and the composition of main carrier gas. The effect of biasing at elevated temperatures (temperature bias test) and post deposition annealing on the surface charge density of the systems were also studied. In general, regardless of the dopant type and the substrate orientation negative charge was always found in the insulator of MAS samples. On the other hand, positive charges were found frequently in the insulator of MAOS samples. Only occasionally the negative charge was observed in the insulator of MAOS system. This is believed due to the nature of the $Al_2O_3-SiO_2$ interface.

13.1 Effect of Substrate Temperature on the Surface Charge Density N_{FB} of MAS System

Figure 17 shows a typical C-V curve of the Al_2O_3 films deposited at temperatures higher than 800°C. As can be seen, in contradiction to the findings in the MOS (metal $-SiO_2-Si$) system in which the insulator is positively charged, the flat band voltage, V_{FB}, in the MAS system is positive, indicating the insulator is that negatively charged, and the silicon surface is positively inverted. This is in agreement with the findings of Aboaf[7] and Matsushita and Koga.[8] Generally, except that of the Al_2O_3 films deposited below 750°C, the C-V curves of Al_2O_3 films deposited at higher temperatures are fairly stable at room temperature and exhibit only minor trapping type hysteresis.

Table III presents the calculated data of flat band charge densities N_{FB} of Al_2O_3 films deposited at temperatures from 750° to 1050°C. It appears that in the temperature range from 800°C to 1050°C, N_{FB} is more or less dependent on substrate temperature. The positive flat band voltages are indicative of negative charges in the film and positive charge on the silicon surface. This is so-called-"P-type invert" of the silicon surface as just mentioned.

13.2 Effect of the $CO_2/AlCl_3$ Mole Ratio

Table IVsummarizes the V_{FB} and N_{FB} data of the Al_2O_3 films deposited in a reactant gas containing different $CO_2/AlCl_3$ mole ratio. Since hydrogen was used as main carrier gas, any changes of $CO_2/AlCl_3$ mole ratio will correspondingly alter the concentration of CO_2 in the gas phase, consequently affecting the kinetics of water formation.

As a predominant rate controlling factor for film growth, the kinetics of water formation may significantly affect film properties. This study was con-

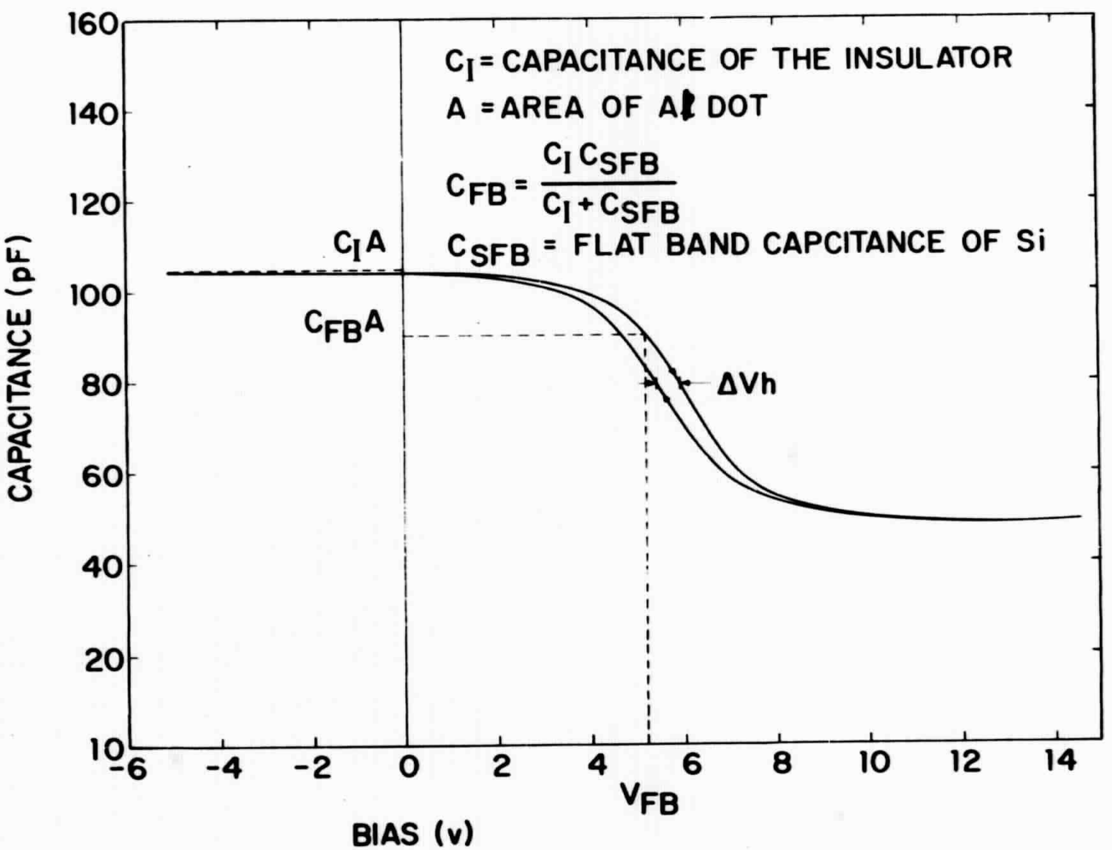

Fig. 17. A typical C-V curve of pyrolytic Al_2O_3 film (900°C) on P^- <100> Si wafer.

TABLE III. Effect of Substrate Temperature on N_{FB} **

Sample	Wafer	Substrate Temp. (°C)	V_{FB}(V)	N_{FB}($1/cm^2$)
21-8	P^- (100)	750	+4.5	12.7×10^{11} *
10-6	N^- (111)	800	+1.7	7.4×10^{11}
15-6	N^- (100)	850	+2.92	8.4×10^{11}
19-8	P^- (100)	950	+3.6	11.0×10^{11}
17-6	P^- (100)	1050	+2.8	8.7×10^{11}

* C-V curve shifts readily at room temperature. The inaccuracy of N_{FB} is high for films deposited at 750°C.

** Flow rate: H_2 (main carrier gas) = 20 l/min, $H_2/AlCl_3$ = 150 cc/min., CO_2 = 400 cc/min.

TABLE IV. Effect of $CO_2/AlCl_3$ Mole Ratio on N_{FB}.

A. Al_2O_3 Films Deposited at 750°C.

Sample	$CO_2/AlCl_3$	$V_{FB}(V)$	$N_{FB}(1/cm^2)$
21-8	310	+4.5	$+12.7 \times 10^{11}$
22-6	248	-0.52	-1.82×10^{11}
23-6	205	-0.52	-1.80×10^{11}
24-6	154	-4.6	-17.0×10^{11}
25-6	145	-0.65	-2.0×10^{11}

B. Al_2O_3 Films Deposited at 900°C.

Sample	$CO_2/AlCl_3$	$V_{FB}(V)$	$N_{FB}(1/cm^2)$
42-7	18.5	+1.95- +2.15	$+5.33- +5.85 \times 10^{11}$
65-7	24.6	+2.28	$+5.46 \times 10^{11}$
45-7	40.0	+1.95- +2.67	$+4.6- +5.92 \times 10^{11}$
46-7	49.3	+3.25- +3.8	$+6.2- +7.2 \times 10^{11}$
47-7	61.7	+3.9- +4.36	$+8.13- +9.2 \times 10^{11}$
48-7	92.5	+5.72- +6.11	$+13.0 - + 13.7 \times 10^{11}$
49-7	123.0	+0.65- +2.6	$+13.0 - + 49.4 \times 10^{11}$

ducted at 750° and $900^{o}C$. Only limited data are available for comparison. It appears that at $750^{o}C$ there is no definite correlation between flat band charge density and the $CO_2/AlCl_3$ ratio varying from 145.1 to 310.1 (Table IVA). For films prepared at $900^{o}C$, N_{FB} increases steadily with increasing $CO_2/AlCl_3$ mole ratio (Table IVB). The charge density is generally related to the degree of film imperfection; films having more imperfection should exhibit greater charge density. This is probably true for Al_2O_3 films prepared with a large $CO_2/AlCl_3$ mole ratio.

13.3 Effect of the Main Carrier Gas on N_{FB}

Based on the experimental results, it was found that partial substitution of A for H_2 as the main carrier gas has drastically reduced the N_{FB} of the MAS samples. As shown in Table V, when film was deposited in a main carrier gas having H_2 content less than 15%, the N_{FB} of MAS sample was as low as $10^{10}/cm^2$. When the H_2 content in the main carrier gas exceeded 20%, the N_{FB} of the Al_2O_3 film was increased by one order of magnitude. The effect of the type of wafer on N_{FB} was also noticeable in using A as the main carrier gas. Results also strongly indicate that the Al_2O_3 film on P-type wafer has a smaller N_{FB} than that on a N-type wafer.

13.4 Flat Band Voltage and Charge Density of MAOS Samples

The flat band voltage and charge densities of MAOS samples were measured. The results are presented in Table VI. The composite layer of Al_2O_3 over low temperature pyrolytic SiO_2 exhibits the highest N_{FB}, while the Al_2O_3 over in-situ SiO_2 composite film has the lowest N_{FB}. With the exception of one sample, the flat band voltages of all the samples containing composite films of Al_2O_3 over thermally grown SiO_2 were negative. The charge density ranges from 2.0×10^{10} to 2.6×10^{11} per cm^2. As shown in Table VIC, the apparent turn-on voltage, V_T^*, of the composite film (Al_2O_3 over in-situ thermally grown SiO_2) is less than ± 1.0 volts. This makes Al_2O_3 films quite attractive for gate insulator application in FET devices.

13.5 Effect of Temperature-Bias Treatment

Results from preliminary study of the temperature-bias treatment of the Al_2O_3 and the Al_2O_3 over SiO_2 composite films reveal that, the V_{FB} and the N_{FB} of the MAS change only with positive temperature bias, whereas that of the MAOS, with negative temperature bias only (Table VII.).

---

*Obtained by extrapolating the "knee" of C-V curve to absissa.

TABLE V. Effect of A Carrier Gas on N_{FB}.

Sample	Wafer	Carrier Gas H_2(%)	A(%)	V_{FB}(V)	$N_{FB}(1/cm^2)$
102-3	P^- (100)	15	85	-0.26 +0.14V	$-6.8- +3.7 \times 10^{10}$
103-5	P^- (100)	20	80	+2.6	$+6.7 \times 10^{11}$
48-7	P^- (100)	100	0	+5.72 +6.11	$+1.3- +1.37 \times 10^{12}$
102-6	N^- (100)	15	85	-0.26 -0.45	$-6.64- +1.15 \times 10^{11}$
103-4	N^- (100)	20	80	+4.5 +4.9	$+1.2- +1.3 \times 10^{12}$

Note: Deposition condition: substrate temperature = 900°C; $H_2/AlCl_3$ = 500 cc/min; CO_2 = 200 cc/min.

TABLE VI. V_{FB} and N_{FB} of MAOS (Metal-Al_2O_3 - SiO_2-Si) Structures.

A. Al_2O_3 over Pyrolytic SiO_2*.

Sample	Wafer	Film (Å) SiO_2	Film (Å) Al_2O_3	Sub.Temp. (°C)	V_{FB}(V)	N_{FB}($1/cm^2$)
88	P^- 100	1200	1000	900	-7.0	-1.3×10^{12}
60-5	P^- 100	1900	1000	1050	+4.6	$+7.0 \times 10^{11}$

*Deposition temperature 475°C.

B. Al_2O_3 thermally SiO_2.

Sample	Wafer	Film (Å) SiO_2	Film (Å) Al_2O_3	Sub.Temp. (°C)	V_{FB}(V)	N_{FB}($1/cm^2$)
40	N^- 100	4000	1200	900	+0.25	$+2.1 \times 10^{10}$
55-7	P^- 100	4000	1200	900	-2.6	-2.6×10^{11}
65-4	N^- 100	500	2000	900	-1.3	-1.5×10^{11}
65-2	N^- 100	1000	2300	900	-1.95	-1.8×10^{11}
86-9	N^- 100	4500	1500	900	-3.3	-2.6×10^{11}
87-5	N^- 100	780	1500	900	-1.04	-2.0×10^{11}

C. Al_2O_3 over in-situ SiO_2* (substrate temperature 900°C)

Sample	Wafer	Film (Å) SiO_2	Film (Å) Al_2O_3	V_T(V)	V_{FB}(V)	N_{FB}($1/cm^2$)
91-2	P^- 100	500	500	+0.6	+0.2	$+4.76 \times 10^{10}$
91-5	P^- 111	500	500	+0.01	-0.4	-1.05×10^{11}
94-3	P^- 100	500	3000	+1.5	-0.3	-4.4×10^{10}
94-4	P^- 111	500	3000	-1.6	-2.4	-3.4×10^{11}
95-5	P^- 100	1000	500	+0.4	-0.14 +0.12	$-2.8- +2.0 \times 10^{10}$
95-3	P^- 100	1000	500	+0.01	-0.52	-9.5×10^{10}

*Dry oxygen at 1000°C.

TABLE VII. Effect of Temperature - Bias Treatment.

Sample	Wafer	Film (Å) SiO_2	Al_2O_3	Temp. Bias	$\Delta V_{FB}(V)$	$\Delta N_{FB}(1/cm^2)$
65-7	N^- (100)	0	2000	-	0	0
				+	-3.04	-7.4×10^{12}
65-4	N^- (100)	500	2000	-	+2.6	$+6.2 \times 10^{11}$
				+	0	0
65-2	N^- (100)	1000	2300	-	-1.6	-1.6×10^{11}
				+	0	0

Note: "-" -30 volts at 200°C for 30 min in dry N_2
"+" +30 volts at 200°C for 30 min in dry N_2

13.6 Effect of Post Deposition Heat Treatment

The objective of post-deposition heat treatment is to make the film more homogeneous, to reduce the surface state charge and to minimize the space charge density. In some instances the chemical stoichiometry might even be improved and lattice defects can be reduced. This has been demonstrated in the case of thermally grown SiO_2 layer on silicon. In Al_2O_3 -SiO_2 composite film the interfacial structure as well as its stability becomes extremely important. Thus we have conducted some limited experiments studying the effects of V_{FB} and N_{FB} resulting from post-deposition heat treatment.

Two sets of samples, each consisting of N^- (100), N^- (111), P^- (100) and P^- (111) silicon wafers, were annealed in nitrogen at 550°C and 800°C for half an hour, respectively. These temperatures were chosen so that no possible structural transformation of Al_2O_3 film from γ to α phase would occur during annealing. This structural transformation was noted to take place at approximately 950°C. (Sec. 7.0) After annealing, samples were cooled in air. Metal-Insulator-Si (MIS) capacitors were then made and C-V curves were plotted. The flat band voltage, V_{FB}, deduced from the C-V curve of the samples, before and after annealing, are presented in Table VIII. In the same table, the voltage shift of the C-V curve due to surface charge only, V_q, and its change due to annealing ΔV_q, are also presented.*

As noted in Table VIII, after 800°C annealing, the change of V_q values in the MAOS system appears larger than that in the MAS system where the change of surface charge in the Al_2O_3 films deposited on (100) wafers appears higher as compared with that on the (111) wafers. Furthermore, as result of 800°C annealing, the silicon surface of the MAS samples of (100) orientation tends to be more P^- inverted. However, annealing in N_2 caused an increase in the positive charge in the insulator in the MAOS system which is different with the findings in the MOS (metal-SiO_2-Si) system.[9,10] The reduction of the surface charge in the MOS system (or a decrease of positive charge in the insulator) was interpreted as the result of a modification in the structure of the SiO_2-Silicon interface.[11,12] Since the same type of atomic bonding exists across the insulator-silicon interface in both the MAOS and MOS systems, a reduction of the surface charge should also be observed in the MAOS system if annealing in N_2 exerted the same effect on the MAOS system as it did on the MOS system. Therefore, in the MAOS system the increase of surface charge indicates that a different charge modifying mechanism was functioning. However, due to limited data available, the findings can not be more conclusive at this time. More exploratory work in this area would be valuable to better understand the characteristics of Al_2O_3 over SiO_2 composite film for the gate insulator of IGFET.

---

* See Appendix A

TABLE VIII. Effect of Post Deposition Heat Treatment on Surface Property of MAS and MAOS Samples.

A. MAS Samples

Sample	Wafer	Insulator	Heat Treatment*	V_{FB}(V)	V_Q(V)	ΔV_Q^{**}(V)
146-4-A	n^- (100)	Al_2O_3	no	+ 1.13	+1.45	-
146-4-B	n^- (100)	Al_2O_3	a	+ 1.38	+ 1.70	+ 0.25
146-4-C	n^- (100)	Al_2O_3	b	+ 2.13	+ 2.45	+ 1.00
146-1-A	n^- (111)	Al_2O_3	no	+ 0.2	+ 0.52	-
146-1-B	n^- (111)	Al_2O_3	a	+ 0.05	+ 0.37	- 0.15
146-1-C	n^- (111)	Al_2O_3	b	- 0.2	+ 0.12	- 0.40
146-2-A	p^- (100)	Al_2O_3	no	+ 0.66	+ 1.58	-
146-2-B	p^- (100)	Al_2O_3	a	+ 1.20	+ 2.10	+ 0.52
146-2-C	p^- (100)	Al_2O_3	b	+ 1.27	+ 2.17	+ 0.59
146-3-A	p^- (111)	Al_2O_3	no	- 2.17	- 1.27	-
146-3-B	p^- (111)	Al_2O_3	a	- 2.30	- 1.40	- 0.13
146-3-C	p^- (111)	Al_2O_3	b	- 2.11	- 1.21	+ 0.06

Note: * a = annealed at 550°C for 30 minutes in N_2

b = annealed at 800°C for 30 minutes in N_2

no = As-deposited

** ΔV_Q = V_Q of sample "B" or "C" minus V_Q of sample "A".

B. MAOS Samples

Sample	Wafer	Insulator	Heat Treatment*	V_{FB}(V)	V_Q(V)	ΔV_Q^{**}(V)
160-C	p^- (100)	500 Å Al_2O_3 + 400 Å SiO_2	no	- 0.10	+ 0.80	
160-B	p^- (100)	500 Å Al_2O_3 + 400 Å SiO_2	a	- 0.95	- 0.05	- 0.85
160-A	p (100)	500 Å Al_2O_3 + 400 Å SiO_2	b	- 1.15	- 0.30	- 1.1[illegible]
161-1-A	n^- (100)	640 Å Al_2O_3 + 360 Å SiO_2	no	+ 0.40	+ 0.72	
161-1-B	n^- (100)	640 Å Al_2O_3 + 360 Å SiO_2	a	+ 0.45	+ 0.75	+ 0.03
161-1-C	n^- (100)	640 Å Al_2O_3 + 360 Å SiO_2	b	- 0.45	- 0.13	- 0.85
161-4-A	n^- (111)	640 Å Al_2O_3 + 360 Å SiO_2	no	- 0.90	- 0.58	
161-4-B	n^- (111)	640 Å Al_2O_3 + 360 Å SiO_2	a	- 0.75	- 0.43	+ 0.15
161-4-C	n^- (111)	640 Å Al_2O_3 + 360 Å SiO_2	b	- 1.35	- 1.03	- 0.45
161-2-A	p^- (100)	640 Å Al_2O_3 + 360 Å SiO_2	no	- 0.10	+ 0.80	
161-2-B	p^- (100)	640 Å Al_2O_3 + 360 Å SiO_2	a	-0.15	+ 0.75	- 0.05
161-2-C	p^- (100)	640 Å Al_2O_3 + 360 Å SiO_2	b	-0.90	+ 0.00	- 0.80
161-3-A	p^- (111)	640 Å Al_2O_3 + 360 Å SiO_2	no	- 1.20	- 0.30	
161-3-B	p^- (111)	640 Å Al_2O_3 + 360 Å SiO_2	a	- 1.15	- 0.20	+0.10
161-3-C	p^- (111)	640 Å Al_2O_3 + 360 Å SiO_2	b	- 1.95	- 1.05	- 0.75

Note * Same meaning as in the note of Table I Part A.

** Same meaning as in the note of Table I Part A.

14.0 APPLICATION OF COMPOSITE Al_2O_3-SiO_2 FILM IN IGFET AS GATE INSULATOR

14.1 Device Wafer Fabrication

In order to investigate the actual performance and merits of Al_2O_3-SiO_2 gate insulator in integrated circuits applications, a test device of one-bit shift register, n-channel FET circuit, designed previously[15], had been used. Each circuit is located 0.032" apart, and consists of six FET, essentially of a flip-flop type. The circuit was so designed that each FET can be individually tested. The circuit has an overall size of 0.018" x 0.020". Figure 18 shows the circuit diagram and Fig. 19 represents its actual layout.

In preparation the devices P^- ⟨100⟩ silicon wafers, chemical-mechanical polished,were used. The wafers used for the first two batches of device wafers had resistance of 2Ω-cm. Approximately 5000Å SiO_2 were first thermally grown on the well cleaned wafers, and the source and drain window patterns were carefully opened by conventional photo-etch methods. Phosphorus diffusion for the source and drain was conducted in an open tube at 970°C. The junction depth of source and drain was controlled at approximately 1.5μ and the sheet resistance after phosphorus diffusion was approximately 5Ω/□. As indicated before, the thin composite film of Al_2O_3 -SiO_2 has a low surface charge density and low apparent turn-on voltage of less than 1.0V. Therefore, in the initial study, a composite film of 500Å Al_2O_3 over 500Å SiO_2 was arbitrarily chosen for gate insulator in the intended IGFET device preparation.

The first two batches of one-bit-shift register device wafers were completed in late March. Unfortunately, due to excessive circuit shortings and leakages found in most of the devices, they were discarded. A third batch of device wafer was then initiated observing rigid precautions in every step of processing, and this batch was completed in late April. In fabricating the third batch of the devices, 14Ω-cm P^- (100) Si wafers were used. The N^+ regions of the discrete device were formed by open tube phosphorous diffusion at 970°C. In these two regions, the surface concentrations of phosphorous C_o, are both 3.8×10^{20} atoms/cm^3 with a depth of 1.5μ. The composite gate insulator in this case consisted of 500Å of Al_2O_3 over 500Å in situ SiO_2 grown at 1000°C. During the device wafer fabrication, some difficulties such as mask alignment, gate region etching, etc. were encountered. Excessive undercuts often resulted from overetching which produced leaky devices.

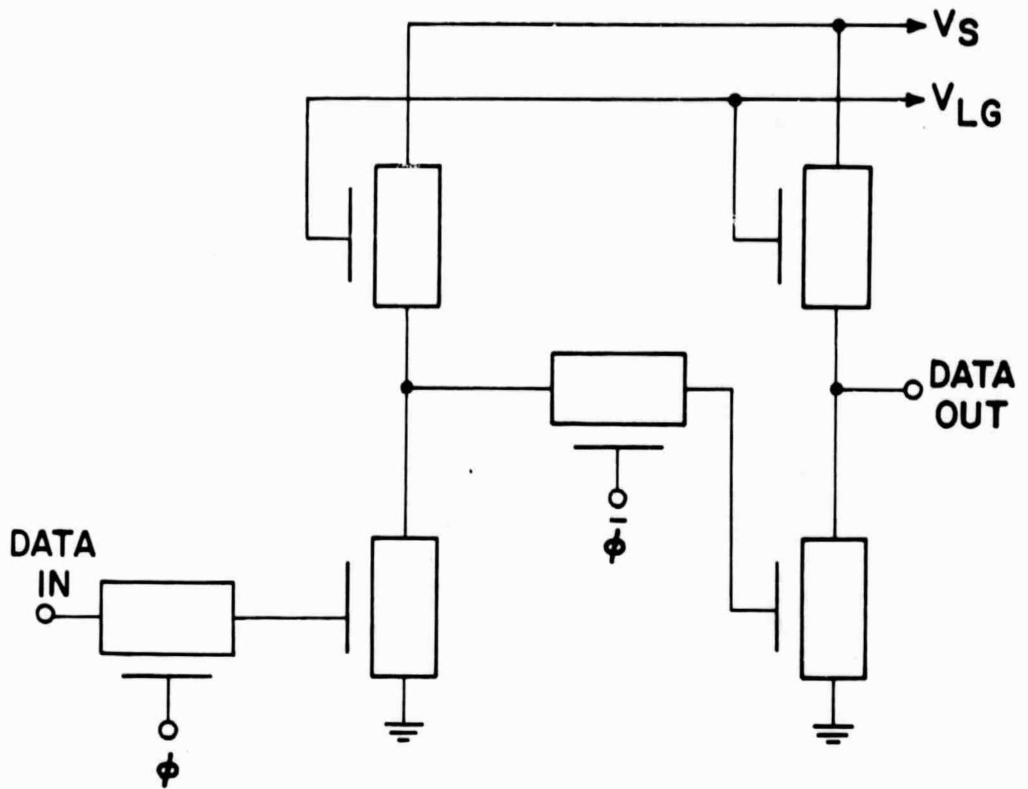

Fig. 18. Circuit diagram of one-bit shift register circuit. (Ref. 15).

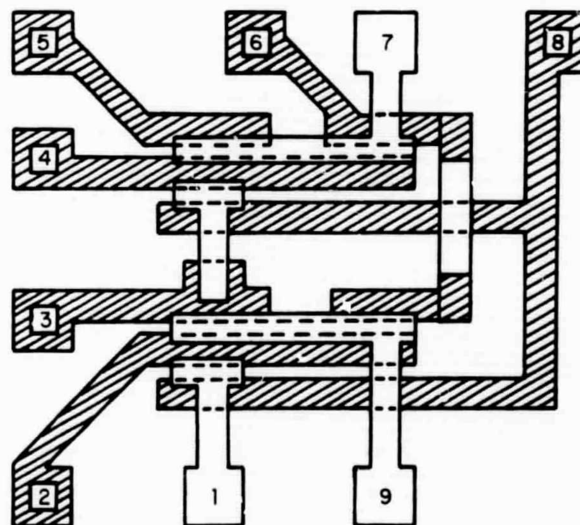

Fig. 19. Mask layout for one-bit shift register circuit. (Ref. 15).

14.2 Performance of Al_2O_3-SiO_2 Gate IGFET

The set-up for dc characteristic measurement is shown in Fig. 20. A Textronic type 575 transistor curve tracer was used for tracing the I_d versus V_d curves. The source of the discrete FET was always grounded while the substrate was either grounded (zero substrate bias) or negatively biased by a constant dc voltage supply. All the FETs were normally at the "on" stage when the substrate was grounded (zero substrate bias, i.e., $V_{sub.} = 0.$) Figure 21a shows a typical family of I_d vs V_d curves obtained from a discrete FET in the circuit where the gate voltage V_g was increased 0.2 V per step. Figure 21b through 21c show the families of curves of I_d vs V_d of the same device but at various substrate bias levels (V_{sub}). As expected, a larger turn-on voltage or threshold voltage, V_t, was needed to turn on the device when the substrate was more negatively biased. Data on the transconductance* as shown in Table IX was calculated from the I_d vs V_d curves according to the following equation, using a saturation I_d formula.

$$\gamma_m = \left.\frac{\partial I_d}{\partial V_g}\right| V_d = \text{constant}$$

In the same table, the turn-on voltages, V_t, of the device at various substrate bias were also included. The turn-on voltages were obtained by extrapolating the curves of channel conductance vs gate voltage to intercept the abscissa.[13a]

The average experimental value of the dielectric constant of pure pyrolytic Al_2O_3 film (γ-phase, deposited at 900°C), $K_{Al_2O_3}$ obtained in this laboratory is 10.0. Assuming Al_2O_3 and SiO_2 films in the $Al_2O_3 + SiO_2$ composite film (double layer) act as two independent capacitors in series, the "theoretical" dielectric constant, K, can be calculated, using $K_{Al_2O_3} = 10.0$ and $K_{SiO_2} = 3.9$.[13b] K thus obtained is 5.7. Based on this value of K, the effective electron mobility, μ_{eff}, of present $Al_2O_3 + SiO_2$ gate FET with substrate grounded was calculated from its transconductance and is found to be 518 cm^2/v-sec. The ratio of the effective electron mobility of present Al_2O_3 - SiO_2 gate FET and that of intrinsic silicon, μ_{eff}/μ_{bulk} is therefore 0.385. (μ_{bulk} = 1350 cm^2/v-sec. [Ref. 13]). This is slightly smaller than the finding of Leistiko, et al[14] from a MOST. However, the experimental value of K of the composite film of comparable thickness (500Å Al_2O_3 + 500Å SiO_2) was found to be 5.0 from the C-V measurement of a MAOS capacitor. If this "measured" K value was used, the calculated μ_{eff} for the same FET will then be 590 cm^2/v-sec. This is equivalent to a μ_{eff}/μ_{bulk} ratio of 0.438 which is in agreement with the maximum μ_{eff}/μ_{bulk} ratio found by Lestiko, et al. in a MOST.

Direct comparison with n-channel SiO_2 gate and/or $Si_3N_4 + SiO_2$ gate FETs of comparable geometric dimensions and gate insulator thickness is not possible since no data from the latter is available.

---

*Taken at $V_g - V_t = V_{dsat}$ = 2.1 volt for V_{sub} = 0.0 volt.

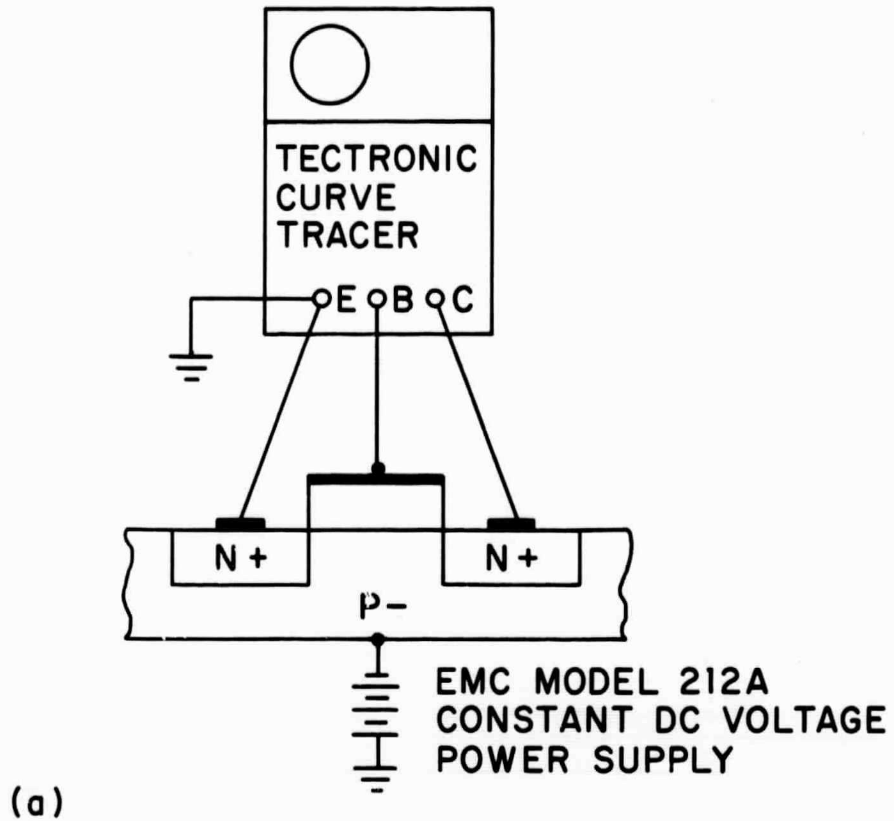

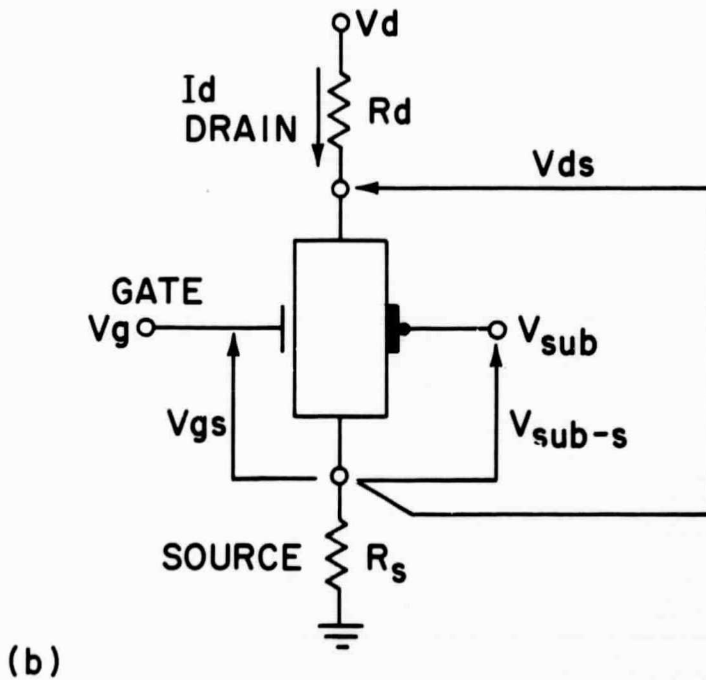

Fig. 20. (a). DC measurement setup.
(b). Grounded-source characteristics of the IGFET.

PRECEDING PAGE BLANK NOT FILMED.

TABLE IX. Transconductance of $Al_2O_3 - SiO_2$ gate IGFETs in IC 199 circuit.

V_{sub}(V)	0.0	- 5.0	- 10.0	- 15.0
γ_m(μmhos)	550	500	450	450
V_t (V)	- 0.9	- 0.55	- 0.14	+ 0.23

Device geometric dimensions and fabrication parameters can affect the I_d--V_d characteristic, which in turn affect the transconductance and charge mobility to some extent. To further verify the results obtained from the above circuit, 12 additional experimental device wafers were processed and evaluated. The device patterns on these test wafers have different device geometrical dimensions and were previously designed by IBM Research Center (Yorktown Heights) for its own development purpose. They were made available as a test vehicle for composite Al_2O_3-SiO_2 gate insulator evaluation through the courtesy of IBM's T.J. Watson Research Center.

The I_d--V_d characteristics of the fabricated devices were measured by an automatic testing system. The turn on voltage, V_t, and the normalized transconductance of the FETs of two different ratios of channel width over channel length, W/L, are shown in Table X. The turn-on voltages of the FETs, with substrate properly biased, were the gate voltages, V_g, at I_d of 30 μA, whereas the normalized transconductance, γ_n, is defined as

$$\gamma_n = \mu_{eff} (K_{ox} \epsilon_o / t_{ox}) \qquad (2)$$

where

μ_{eff} = effective charge mobility

K_{ox} = dielectric constant of gate insulator

ϵ_o = permitivity of free space

t_{ox} = thickness of gate insulator

The γ_n shown in Table X were calculated from the I_d - V_d data of corresponding device, substrate biased at -7.0v according to Eq. (3) with V_d and I_d chosen at

V_d = 0.5V, I_d = 120 μA for devices having W/L = 8, and

V_d = 0.5V, I_d = 60 μA for devices having W/L = 11

$$\gamma_n = \frac{I_d}{V_d \left(V_g - V_t - \frac{V_d}{2}\right) \frac{W}{L_{eff}}} \qquad (3)$$

when

I_d = Drain current

V_d = Drain voltage

V_t = Turn-on voltage

W = Channel width

L_{eff} = Effective channel length

TABLE X. DC characteristics of $Al_2O_3 + SiO_2$ Gate IGFET.

Channel width	Gate Total Thickness ($Al_2O_3 + SiO_2$) (Å)	for $V_{sub} = -3V$	for $V_{sub} = -7V$	γ_n (1)
11	500	0.68–0.93	0.95–1.25	30–36
8	500	0.70–0.90	1.00–1.25	30–39
11	1000	0.90–1.50	1.54–2.03 (2)	20–22 (3)
8	1000	0.94–1.53	1.60–2.00	21–23

Note: (1) γ_n = normalized transconductance = $\mu_{eff} \, (\epsilon_o \epsilon_{ox} / t_{ox})$

(2) ~ 2.0V for comparable SiO_2 gate FET

(3) ~ 18 for comparable SiO_2 gate FET

As can be seen in Table X, the transconductance of present 1000Å Al_2O_3 + SiO_2 gate FETs is approximately 22% higher than that of the comparable SiO_2 gate FET of same gate thickness, although its turn-on voltage is more or less the same, as compared with the SiO_2 gate FET. Using the experimental dielectric constant of the gate insulator, i.e., K = 5.0, the average electron mobility, calculated from the normalized transconductance, was 496 cm^2/v-sec. in present 1000Å Al_2O_3 + SiO_2 gate FET, with substrate biased at -7.0 volts. This value is approximately 97% of that of a comparable 1000Å SiO_2 gate FET and is approximately 0.368 of the electron mobility in intrinsic bulk silicon.

In summary, results show that in an Al_2O_3 + SiO_2 gate FET, the electron mobility in the channel is more or less maintained at the same level as that in a SiO_2 gate FET, whereas its transconductance is somewhat higher. This presumably is attributed to the fact that the "measured" dielectric constant of the composite gate insulator is smaller than the "theoretical" value. Results of post-deposition heat treatment (Sec. 13.6 of this report) show that a change in the characteristics of the SiO_2-Si interface in MAOS structure was resulted from the existance of Al_2O_3-SiO_2 interface in the insulator. It is plausible to suggest that Al_2O_3 -SiO_2 interface has appreciably modified the dielectric characteristics hence the dielectric constant of the composite film. Additional possible advantages of using Al_2O_3 -SiO_2 composite film as gate insulator are : (1) improved device reliability due to the prevention of sodium migration toward the oxide-silicon interface and (2) reduced the danger of gate electrode shorting due to the high resistance of Al_2O_3 to further reaction with the metal.

15.0 CONCLUSIONS

A. Thin film of γ - Al_2O_3 have been successfully prepared by reacting the $AlCl_3$ vapor with CO_2 and H_2 at temperatures up to 900°C. Important deposition parameters including temperature, feed rate and gas composition had been investigated. The growth mode, morphology, structure and fundamental properties of the films prepared under various conditions were carefully studied. In this unique chemical deposition system, the rate of water vapor formation apparently becomes a key controlling factor in the film growth rate.

B. The masking ability of Al_2O_3 film against diffusion of common dopants was not very attractive but the film has excellent Na retaining ability in comparison with SiO_2 film.

C. The interfacial charge characteristics of MAS (Al-Al_2O_3-Si) structure was found to be different from the MOS (Al-SiO_2-Si) structure. In MAS structure the insulator exhibits negative charge,while in MOS structure the insulator is characterized with positive charge.

D. Homogeneous, single phase γ - Al_2O_3 film has been found to be satisfactory for microcircuits application, in particular when combined with SiO_2 to form a composite gate insulator for FET device.

E. It has been observed that high temperature post-deposition heat treatment can improve the surface charge density of MAS and MAOS structures. Present results suggest that with suitable heat treatment, it is possible to tailor the surface charge density of the insulating film to meet the requirements of the FET.

F. Based on the results obtained from a limited study, it is evident that the composite film of $Al_2O_3 + SiO_2$ can be a satisfactory material for IGFET as a gate insulator. $Al_2O_3 + SiO_2$ gate FETs fabricated in this experiment have shown higher transductance than a single layer SiO_2.

16.0 RECOMMENDATIONS

From this investigation the gate insulator of an FET device consisting of a composite film of Al_2O_3 over SiO_2 has proven certain advantages. To further optimize the device performance, additional studies should include:

A. Investigating the interfacial charge properties of Al_2O_3-Si and Al_2O_3-SiO_2-Si structures with respect to the following parameters.

1. Other Al-containing source materials for Al_2O_3 film deposition.

2. Variation of feed compositions.

3. Variation of thickness ratio of Al_2O_3 over SiO_2 in the Al_2O_3-SiO_2-Si structure.

4. Post-deposition heat treatment under different gas atmospheres.

5. Temperature-bias treatment.

6. Important dopants for Al_2O_3 film.

B. Life testing on reliability and stability of the device.

C. Characterization based on the results from selected property measurements.

17.0 NEW TECHNOLOGY

After a deligent review of the work performed under this contract, the following are considered to be the innovations and improvements in the development of pyrolytic polycrystalline aluminum oxide film as useful material for microelectronics.

A. The success of this project proves the feasibility of large scale production of homogeneous single phase pyrolytic Al_2O_3 on any kind of substrate in a RF horizontal system in the temperature range of 700°C to 950°C.

B. A new design and construction of $AlCl_3$ evaporation apparatus will enable the evaporation of $AlCl_3$ at a controllable and steady rate.

C. The use of a gas mixture of H_2 and inert gas (A or He) at certain proportion for H_2 as main carrier gas makes it possible to deposit Al_2O_3 film with low surface charge density.

D. The application of composite pyrolytic Al_2O_3 over thermal SiO_2 film in n-channel IGFET as gate insulator tends to increase the device gain.

ACKNOWLEDGEMENTS

The authors wish to thank Messrs, J. Hollis, E. Gorey, G. Walker, J. Woods, R. Baker, R. Elma, C. Johnson, V. Richardson, A. Smith and W. Patterson for their assistance in various experimental works and measurements. The authors are also indebted to Drs. D. R. Young and L. V. Gregor for their critical review and comments on the last portion of this report.

APPENDIX A

By conventional definition, the flat band voltage, V_{FB}, resulted from the effective surface charge, Q_{eff}, and the effect of the work function difference between the metal and semiconductor, ϕ_{MS}; i.e.,

$$V_{FB} = -Q_{eff}/C_i + \phi_{MS}$$

where

$Q_{eff} = Q_{ox} + Q_{ss}$ = effective surface charge

C_i = capacitance of insulator

ϕ_{MS} = work function difference between metal and semiconductor

Therefore

$Q_{eff}/C_i = V_q$ represents the voltage shift of the C-V curve due to the effective surface charge.

Then

$$V_{FB} = -V_q + \phi_{MS}$$

knowing ϕ_{MS}, V_q may be calculated from V_{FB}.

V_{FB} and change in V_{FB} are commonly used to measure the surface charge and the change in surface charge of the MIS structure. However, due to the presence of ϕ_{MS}, the sign of V_{FB} that is obtained directly from the C-V curve does not necessarily represent the sign of the surface charge existing in the insulator. To represent the surface charge in the insulator directly and faithfully, V_q and the change in V_q were used in this report in studying the effect of post-deposition annealing. The values of V_q presented in Table VIII were calculated from corresponding V_{FB}'s by assuming $\phi_{MS} = -0.9V$ for the P^- wafer and $-0.23V$ for the N^- wafer used in this investigation. (Ref. 11).

18.0 REFERENCES

1. V. Y. Doo and D. Kerr, Final Report, NASA Contract NAS12-105, April 30, 1967.

2. Handbook of Physics and Chemistry 45th Ed. (1965).

3. A. F. Wells, "Structural Inorganic Chemistry" 3rd Ed. Oxford, 1962.
   H. Thibon et al. Bull. Soc. Chem. 18, 384 (1951).
   H. C. Stumpf et al. Ind. Eng. Chem. 42, 1398 (1950).

4. L. J. Harris, Opt. Soc. Amer. 45, 27 (1955).

5. R. P. Esch, IBM, Private communication.
   Edward G. Brame, Jr. et al., J. Inorg. Nucl. Chem. 5, 48 (1957).

6. A. S. Grove, B. E. Deal, E. H. Snow and C. T. Sah, Solid State Electronics 8, 145 (1965).

7. J. A. Aboaf, J. Electro Chem. Soc. 114, 948 (1967).

8. M. Matusshita and Y. Koga, Electrochem. Soc. Meeting, Spring 1968, Abstract No. 90.

9. F. R. Badock and D. R. Lamb, Int. J. Electronics 24, 1, (1968).

10. D. R. Lamb and F. R. Badock, Int. J. Electronics 24, 11, (1968).

11. B. E. Deal, et al. J. Phys. Chem. Solids 27, 1873 (1966).

12. B. E. Deal, M. Aklar, A. S. Grove and E. H. Snow, J. Electrochem. Soc., 114, 266 (1967).

13. A. S. Grove, Physics and Technology of Semiconductor Devices, Wiley and Sons, 1967, (a) p. 325, (b) p. 103.

14. V. Leistiko, A. S. Grove and T. Sah, IEEE Trans. Electron Devices, ED-12, 248 (1965).

15. L. V. Gregor, Technical Report AFAL-TR-68-272, Nov. 1968. Air Force Avionic Lab. Air Force System Command, Wright-Patterson Air Force Base, Ohio.

16. S. K. Tung and R. E. Caffrey, Thin Film Dielectrics Edited by Frederick Vratny, pp. 286-296, The Electrochemical Society (1969).

MAN HOUR DISTRIBUTION OF INVESTIGATORS

V. Y. Doo	392
J. Hollis	825
P. C. Li	562
W. Patterson	176
P. J. Tsang	719